

LOCALIZED PHONON-MEDIATED ENERGY TRANSFER
AMONG Eu^{3+} IONS IN SILICATE GLASS-HOSTS

By

SHEENA JACOB

Bachelor of Science

Panjab University

Chandigarh, India

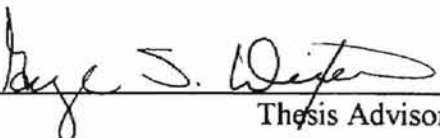
1984

Submitted to the Faculty of the
Graduate College of the
Oklahoma State University
in partial fulfillment of
the requirements for
the degree of
MASTER OF SCIENCE
December, 1995

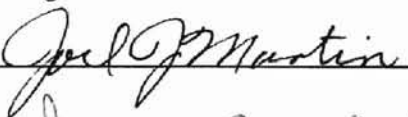
LOCALIZED PHONON-MEDIATED ENERGY TRANSFER

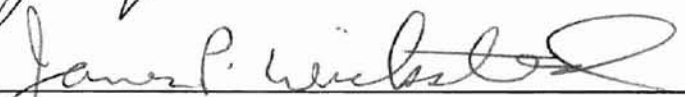
AMONG Eu^{3+} IONS IN SILICATE GLASS-HOSTS


Thesis Approved:



Thesis Advisor







Dean of the Graduate College

ACKNOWLEDGMENTS

I wish to express my gratefulness to Dr. George S. Dixon, research advisor, for his valuable guidance in making this thesis possible. It was a pleasure to work with him. His help, advise and patience is greatly appreciated.

I would like to thank Dr. James P. Wicksted and Dr Joel J. Martin for serving on my committee. I am especially thankful to Dr. Wicksted for providing me with timely laboratory facilities and help.

I want to take this opportunity to thank Dr. Paul Westhaus, for encouraging me to join graduate school, for his academic advise and support.

I owe my sincere thanks to, Michael Furlough, for being with me as a friend and a teacher and educating me on the needed aspects of technical skills, answering my unending train of questions that tried his patience, and yet maintaining his calm throughout the struggle for conducting the experiments successfully.

My heartfelt thanks go out to all my close friends in the Physics department, Anne Georgalas, Steve Willoughby, Jong Eul Lee, Joy Ferris, Ricardo Nieves, John Snodgrass, Cindy Porter, Jeff McCullough, Ulf Nobbman and Yueming He for being considerate, and for instilling confidence in me, at study or otherwise. My special thanks to Abdulatif Hamad and Apollo Mian for the useful discussions, and their companionship while working long hours in the laboratory. Cheryl and Susan, thanks for the years of help with all my office work and at the xerox machine.

My deepest gratitude goes out to my loving parents and brother, George. Their faith in my aptitude in academics motivated me to come back to school. I thank them for their encouragement and support throughout my life, for their practical and moral advise, and especially for the frequent overseas phone calls that immensely helped me to keep my morale up.

TABLE OF CONTENTS

Chapter	Page
I. INTRODUCTION.....	1
The Structure of Glass.....	2
Electron States and Localization.....	4
Localized Phonons in Glass.....	6
Phonon Assisted Energy Transfer.....	7
Fluorescence Spectra of Eu^{3+} in Glass Hosts.....	11
Subject of Investigation.....	12
II. EXPERIMENTAL PROCEDURE.....	13
Samples.....	13
Experimental Setup.....	13
Spectrometer.....	15
Processing Units.....	16
Scan Specifications.....	16
III. RESULTS AND DISCUSSIONS.....	18
Energy Transfer Function $a(t)$	19
IV. SUMMARY AND CONCLUSIONS.....	61
REFERENCES.....	63

LIST OF TABLES

Table	Page
I. Onset of Rising Edge of Low Frequency Boson Peak and of Secondary Peaks	58
II. Onset of Secondary Peaks With Respect to 17316 cm^{-1}	59

LIST OF FIGURES

Figure	Page
1. A two-dimensional representation of quartz (a) crystal lattice, (b) glass network and (c) metal-modified glass.....	3
1.(d) A Bloch type extended-state wavefunction. (e),(f) Disorder induced Anderson localization takes place when W the width of disorder exceeds the overlap bandwidth B . (g) A localized electron state.	5
1.(h) F and D energy levels of Eu^{3+} ions. The widths of the levels indicate the Stark splitting of the crystal field states in glass hosts.	10
2.(a) Experimental set up to study energy transfer. (b) The prism reflects the laser beam through the glass sample producing a vertical fluorescent column in it.	14
3. Spectra of Eu^{3+} in Ca -modified glass 1ms, 3ms, 5ms, 7ms, and 9ms after the excitation pulse; $\lambda_{\text{ex}} = 578\text{nm}$.	23
4. Spectra of Eu^{3+} in Ca -modified glass 1ms, 3ms, 5ms, 7ms, and 9ms after the excitation pulse; $\lambda_{\text{ex}} = 579\text{nm}$.	24
5. Spectra of Eu^{3+} in Ca -modified glass 1ms, 3ms, 5ms, 7ms, and 9ms after the excitation pulse; $\lambda_{\text{ex}} = 580\text{nm}$.	25
6. Spectra of Eu^{3+} in Mg -modified glass 1ms, 3ms, 5ms, 7ms, and 9ms after the excitation pulse; $\lambda_{\text{ex}} = 578\text{nm}$.	26
7. Spectra of Eu^{3+} in Mg -modified glass 1ms, 3ms, 5ms, 7ms, and 9ms after the excitation pulse; $\lambda_{\text{ex}} = 579\text{nm}$.	27
8. Spectra of Eu^{3+} in Mg -modified glass 1ms, 3ms, 5ms, 7ms, and 9ms after the excitation pulse; $\lambda_{\text{ex}} = 580\text{nm}$.	28
9. Spectra of Eu^{3+} in Sr -modified glass 1ms, 3ms, 5ms, 7ms, and 9ms after the excitation pulse; $\lambda_{\text{ex}} = 578\text{nm}$.	29
10. Spectra of Eu^{3+} in Sr -modified glass 1ms, 3ms, 5ms, 7ms, and 9ms after the excitation pulse; $\lambda_{\text{ex}} = 579\text{nm}$.	30

11. Spectra of Eu^{3+} in Sr -modified glass 1ms, 3ms, 5ms, 7ms, and 9ms.....	31
after the excitation pulse; $\lambda_{\text{ex}} = 580\text{nm}$.	
12. Spectra of Eu^{3+} in Zn -modified glass 1ms, 3ms, 5ms, 7ms, and 9ms.....	32
after the excitation pulse; $\lambda_{\text{ex}} = 578\text{nm}$.	
13. Spectra of Eu^{3+} in Zn -modified glass 1ms, 3ms, 5ms, 7ms, and 9ms.....	33
after the excitation pulse; $\lambda_{\text{ex}} = 579\text{nm}$.	
14. Spectra of Eu^{3+} in Zn -modified glass 1ms, 3ms, 5ms, 7ms, and 9ms.....	34
after the excitation pulse; $\lambda_{\text{ex}} = 580\text{nm}$.	
15. Inhomogeneously broadened absorption band spectra for Ca -modified.....	35
glass obtained from Cary05 spectrophotometer at room temperature.	
16. Inhomogeneously broadened absorption band spectra for Mg -modified.....	36
glass obtained from Cary05 spectrophotometer at room temperature.	
17. Inhomogeneously broadened absorption band spectra for Sr -modified.....	37
glass obtained from Cary05 spectrophotometer at room temperature.	
18. Inhomogeneously broadened absorption band spectra for Zn -modified.....	38
glass obtained from Cary05 spectrophotometer at room temperature.	
19. Fluorescence spectra of Eu^{3+} in Ca -modified glass normalized.....	39
with respect to the absorption spectra. $\lambda_{\text{ex}} = 578\text{nm}$.	
20. Fluorescence spectra of Eu^{3+} in Ca -modified glass normalized.....	40
with respect to the absorption spectra. $\lambda_{\text{ex}} = 579\text{nm}$.	
21. Fluorescence spectra of Eu^{3+} in Ca -modified glass normalized.....	41
with respect to the absorption spectra. $\lambda_{\text{ex}} = 580\text{nm}$.	
22. Fluorescence spectra of Eu^{3+} in Mg -modified glass normalized.....	42
with respect to the absorption spectra. $\lambda_{\text{ex}} = 578\text{nm}$.	
23. Fluorescence spectra of Eu^{3+} in Mg -modified glass normalized.....	43
with respect to the absorption spectra. $\lambda_{\text{ex}} = 579\text{nm}$.	
24. Fluorescence spectra of Eu^{3+} in Mg -modified glass normalized.....	44
with respect to the absorption spectra. $\lambda_{\text{ex}} = 580\text{nm}$.	
25. Fluorescence spectra of Eu^{3+} in Sr -modified glass normalized.....	45
with respect to the absorption spectra. $\lambda_{\text{ex}} = 578\text{nm}$.	

26. Fluorescence spectra of Eu^{3+} in Sr -modified glass normalized.....	46
with respect to the absorption spectra. $\lambda_{\text{ex}} = 579\text{nm}$.	
27. Fluorescence spectra of Eu^{3+} in Sr -modified glass normalized.....	47
with respect to the absorption spectra. $\lambda_{\text{ex}} = 580\text{nm}$.	
28. Fluorescence spectra of Eu^{3+} in Zn -modified glass normalized.....	48
with respect to the absorption spectra. $\lambda_{\text{ex}} = 578\text{nm}$.	
29. Fluorescence spectra of Eu^{3+} in Zn -modified glass normalized.....	49
with respect to the absorption spectra. $\lambda_{\text{ex}} = 579\text{nm}$.	
30. Fluorescence spectra of Eu^{3+} in Zn -modified glass normalized.....	50
with respect to the absorption spectra. $\lambda_{\text{ex}} = 580\text{nm}$.	
31. Raman Shift for Mg-, Ca-, Sr-, and Zn-modified glasses, with K-2883,.....	51
K-2885, K-2887, and K-2904, respectively as sample names. Inset	
shows peaks including the low frequency Boson peak.	
32. Time dependence of the energy transfer function defined by Eq. (6) for.....	52
Ca -modified glass.	
33. Time dependence of the energy transfer function defined by Eq. (6) for.....	53
Mg -modified glass.	
34. Time dependence of the energy transfer function defined by Eq. (6) for.....	54
Sr -modified glass.	
35. Time dependence of the energy transfer function defined by Eq. (6) for.....	55
Zn -modified glass.	
36. Time dependence of the energy transfer function for the secondary.....	56
peaks numbered in order of their distance from the excitation peak	
in Ca -modified glass, α being the characteristic time.	
37. Time dependence of the energy transfer function for the secondary.....	57
peaks numbered in order of their distance from the excitation peak	
in Ca -modified glass, α being the characteristic time. (As),(s)	
denote stokes and anti-stokes regions, respectively.	

CHAPTER I

INTRODUCTION

Glass as a disordered medium can host lanthanide ions like Eu^{3+} to facilitate the study of optical properties of these guest ions. The inhomogeneous structural environment on a microscopic scale results in site to site differences in energy levels and radiative and non-radiative transition probabilities of rare earth ions in glass[1]. The broad band excited optical emission spectra consist of the superposition of contributions from individual ions. This is called inhomogeneous broadening.

Laser spectroscopy has been extremely helpful in providing high spectral resolution to probe the structural disorder in glasses. Fluorescence line narrowing (FLN) in glass, a technique to selectively excite a subset of ions with their transition energies resonant with the excitation wavelength, was first studied by Denisov and Kizel (1967). FLN and time-resolved emission spectra of Eu^{3+} were observed in a borate glass, using narrow lines from mercury lamp were used as the excitation source [1].

Experiments conducted by Motegi and Sionoya (1973), emphasized on the vast scope of using laser excited fluorescence for the study of spectroscopic properties of ions in glasses. From their study on energy transfer among Eu ions in an inhomogeneously broadened system, they demonstrated the usefulness of FLN techniques in probing the local field strengths at paramagnetic ion sites in glasses[1].

In the past fifteen years, laser induced FLN has been extensively used to explore other related domains as, electron-phonon coupling, ion-ion interaction, and the effect of these interactions on energy levels in both organic and inorganic glasses.

Recent studies by Gang, Boulon and Powell(1982) [2], and Gang and Powell (1984) [3] on Eu doped glasses using time-resolved site-selection spectroscopy

show a characteristic fluorescence profile that develops a discrete structure with time. They attributed the spectral structure associated with energy transfer to correlation effects within the disorder of the glass network. Dixon [4, 5] using the experimental results of Powell et. al., [2,3] reasoned that phonons localized by the structural inhomogeneities in the medium could also produce these structures.

The significance of such studies lies in being able to obtain information regarding the local structure of the host network [6,7] and/or its excitation spectrum, and in the potential usefulness of glasses for high power laser systems [8].

The Structure of Glass

Glass is a good example of an amorphous solid. Zachariasen (1932) and Warren (1937) gave a description of structure of a glass in terms of *network formers* and *network modifiers*. A crystal lattice is distinguished from a glass network by its translational symmetry. A comparison can be made with the help of two dimensional analogs of quartz crystal (a crystalline form of SiO_2) and quartz glass (an amorphous form of SiO_2) (fig. 1(a),(b)) [9]. Common features of their structures are, fourfold and twofold coordination for Si and O, respectively, constant bond lengths, and, all atoms being bonded - each one to its nearest neighbors. However, the difference between the two lies in the spread of bond angles and a lack of long range translational order in the silicate glass. While SiO_4 tetrahedral is arranged in a regular lattice in quartz crystal (with Si-O-Si bond angle as 109°), quartz glass is built up as an irregular network of tetrahedral with varying Si-O-Si bond angles, the mean value estimated to be $150^\circ \pm 15^\circ$. In both cases an O-ion 'bridges' two Si-ions [10].

Glasses are modified from the above described simple structure to more complicated forms, by fusing the simple network with metal oxides. For divalent metal ions, the O-ion from such an oxide and a bridging O-ion now form two dangling bonds terminated by two non-bridging O-ions bonded to one Si each, thus introducing a discontinuity in the network (fig. 1(c)). This results in interstices that

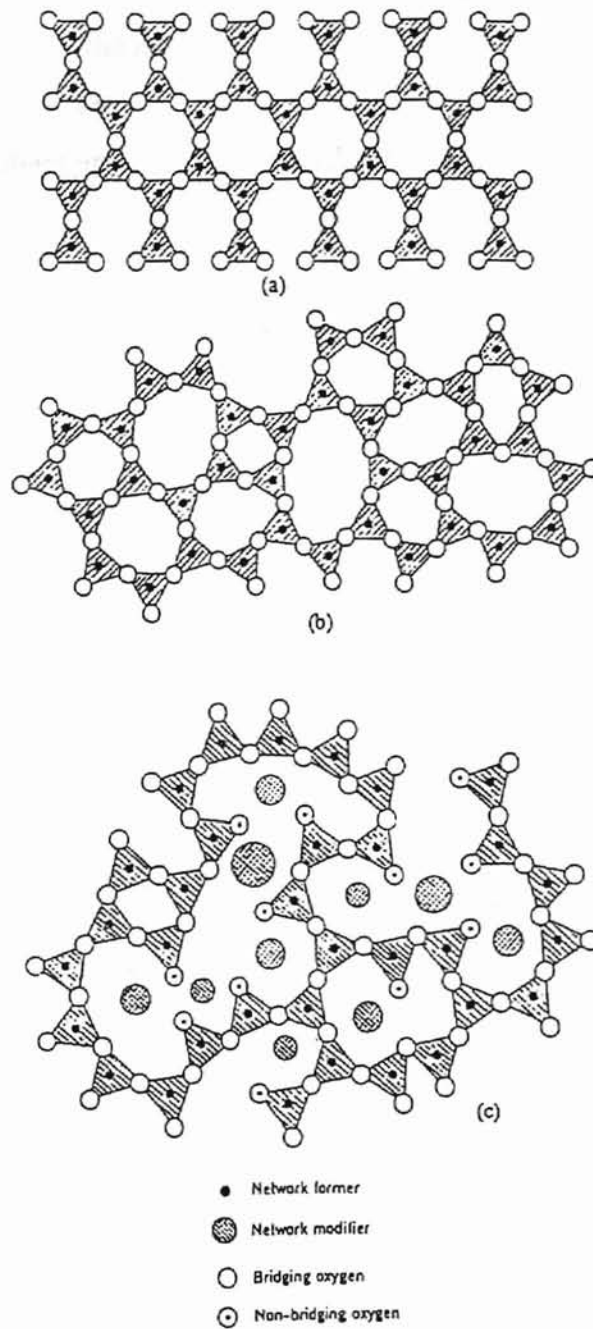


Figure 1. A two-dimensional representation of quartz (a) crystal lattice, (b) glass network and (c) metal-modified glass.

accommodate the metal ions. These cations are named *network modifiers* in contrast to the Si-ions which act as the *network formers*.

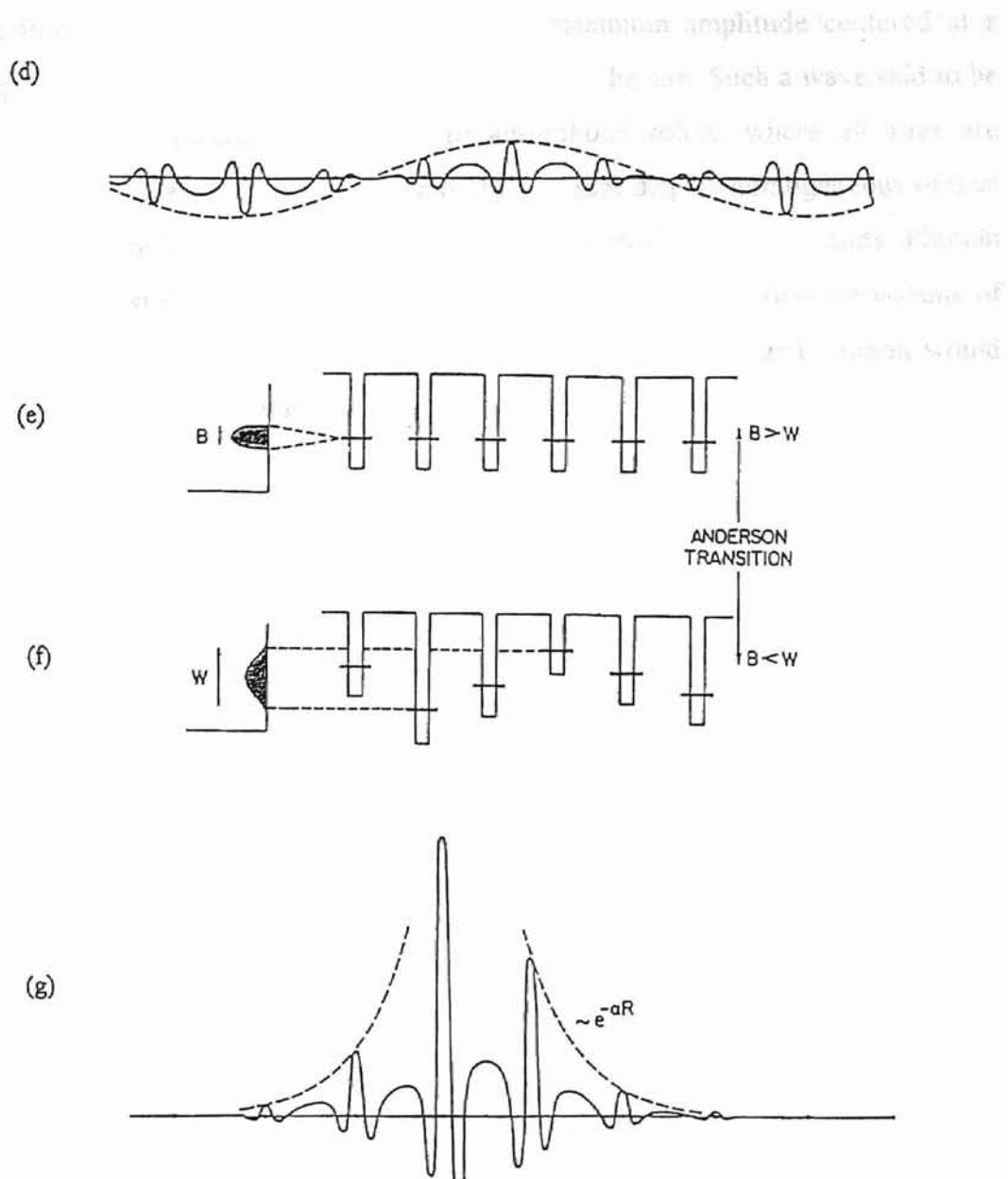
Examples of other network formers are Al_2O_3 , V_2O_5 , P_2O_5 , B_2O_3 , etc. Some commonly used modifiers are oxides of the alkaline earth and the alkali metals, such as, K_2O , CaO , MgO , ZnO , SrO , BaO , etc.

Electron States and Localization

In crystals electron states are described by extended Bloch waves of the form $\phi(\mathbf{k}, \mathbf{r}) = u_{\mathbf{k}}(\mathbf{r})e^{i(\mathbf{k}\cdot\mathbf{r})}$ [11], where \mathbf{k} is the wave vector, \mathbf{r} the spatial coordinate, $u_{\mathbf{k}}(\mathbf{r})$ is a periodic function, i.e., $u_{\mathbf{k}}(\mathbf{r}+\mathbf{R}) = u_{\mathbf{k}}(\mathbf{r})$ that modulates the plane wave part $e^{i(\mathbf{k}\cdot\mathbf{r})}$, and \mathbf{R} is the lattice constant (fig. 1(d)). \mathbf{k} is one of the quantum numbers characterizing each wave, $-\pi/R < k < \pi/R$. Another quantum number is the energy describing the electron state or the band energy $E(\mathbf{k})$, a function of $\hbar\mathbf{k}$, the crystal momentum for each energy band. Electronic wave function in the vicinity of Fermi level E_F are extended, i.e., the wave function has appreciable amplitude throughout the solid. The plane wave envelope (fig. 1(d)) takes several lattice constants \mathbf{R} to form a complete wave of wave vector \mathbf{k} .

On the other hand, a plane wave description of electron states becomes meaningless in glasses because of their structural disorder[10]. Anderson(1958) theorized that disorder-induced localization of electronic states is characteristic of amorphous solids.

Fig. 1(e) shows potential wells representing atomic sites with a single valence electron of each atom occupying, in the isolated atom limit, a bound energy level shown as a horizontal line. This level gives rise to an energy band width B , in an ordered lattice. Fig. 1(f) shows potential wells of varying depths resulting in an energy range W for a topology of spatial fluctuations. Anderson showed through quantum mechanical calculations that when $W > B$, the Bloch function is replaced by wave functions of the form $\sim e^{-\alpha r}$ (fig 1(g)), where α is a parameter called the inverse



localization length. The wave function has its maximum amplitude centered at a small group of atoms, and decays with distance from the site. Such a wave said to be localized. The localization is intrinsic to amorphous solids, where all sites are different from one another. Rare earth modified glasses display homogeneous optical linewidths, owing to the large amplitude vibrational motion of the ligands. Phonon energy $\hbar\omega$ is distributed in the glass in the ratio $\sim l^3/V$, V and l being the volume of the sample and the localization length, respectively[12]. A localized phonon would then have its energy distributed over a much smaller number of atoms as compared with an extended phonon of the same energy indicating a larger amplitude for the localized phonon.

The $E(\mathbf{k})$ band structure representation of electron states is analogous to vibrational modes or phonons. In crystals, phonons with a well defined energy $E(\mathbf{k})$ when interacting

with light form a discrete line spectrum. By contrast, localized phonons of different energies are characteristic of the disorder in amorphous solids. Such phonons, participating in interaction with light, result in inhomogeneously broadened linewidths. Disorder in crystals is due to defects, lattice imperfections and local strain cause an inhomogeneous line broadening of $\leq 1\text{cm}^{-1}$, whereas the same transition in glass would result in a broadening of $\geq 100\text{cm}^{-1}$ [1].

Localized Phonons in Glass

Like electron waves, elastic waves also can be localized by disorder. For example, the glasses under investigation have a composition 0.65SiO_2 , $0.15\text{Na}_2\text{O}$, 0.15MO , $0.05\text{Eu}_2\text{O}_3$, where M is Ca , Mg , Zn , or Sr . Raman scattering studies for these glasses show the onset of low frequency 'boson peak' to be between 14 and 18cm^{-1} . If \mathbf{k} were a good quantum number, then conservation of energy and wave vector would forbid Raman activity except at a few discrete frequencies. The beginning of continuous Raman activity indicates that \mathbf{k} then is no longer a good quantum number characterizing a phonon. For extended phonons \mathbf{k}^{-1} is presumed to

be less than or equal to the correlation length ξ , a measure of disorder in the network. The slightly perturbed extended phonon acquires a finite mean free path Λ such that $\Lambda \gg k^{-1}$, i.e., the phonon is scattered by the inhomogeneities in the density and elastic properties of the network. The Ioffe-Regel condition for the weak scattering description ceases to be valid once k^{-1} becomes comparable to Λ . Thus for phonons the criterion $k\xi \sim 1$ is considered to mark the beginning of the strong scattering regime[13] resulting in phonon localization.

Phonon Assisted Energy Transfer

The rare earth ions introduced in the glass network interact with the local vibrations via the electron phonon coupling. Non-radiative transitions between excited states of two ions 1, 2 separated by energy ΔE_{12} has been treated by Holstein, Lyo and Orbach (HLO)[14]. The HLO method for the energy transfer among optically active ions employs Debye phonons as mediators of the mechanism. Dixon [5] extended the HLO method for the energy transfer process as being due to atomic vibrations resulting from disorder in structure of the system. When structural disorder increases to a critical value such that k^{-1} becomes comparable to the magnitude of density fluctuation in the medium (glass in this case), localization sets in, and is defined in terms of frequency at the mobility edge, ω_{me} . Dixon proposed an enhanced rate of energy transfer when localized phonons near ω_{me} are involved. The one- and two- phonon mechanisms[5, 14] cause rapid transitions and a resultant homogeneous broadening at individual ion sites because of differences in ΔE_{12} , varying local fields, and the nature of vibrational modes.

Considering a transition $|1^*, 2\rangle \rightarrow |1, 2^*\rangle$ [5], for which the energy separation between excited states is ΔE_{12} , the interaction Hamiltonian can be written as $H_I = H_{ep} + H_{ii}$ where H_I is the total interaction Hamiltonian, H_{ep} is the electron-phonon coupling Hamiltonian, and H_{ii} is the ion-ion interaction Hamiltonian. The wave function for the α^{th} at the j^{th} site is given by

$$\phi_{\alpha}(r_j) = \left(\frac{1}{8\pi\rho\xi^3} \right)^{1/2} e^{-(2r_j/\xi)} \quad (1)$$

where ρ is the number density of atoms such that

$$\int |\phi_{\alpha}(r_j)|^2 \rho dV = 1 \quad (2)$$

A particular phonon spectrum is characterized by matrix elements of local strain, and the phonon density of states. The latter is used in evaluating the sum over phonon modes that appear in energy transfer equations. The difference in matrix element of the local strain are:

$$\langle n_{\alpha} - 1 | \varepsilon(1) - \varepsilon(2) | n_{\alpha} \rangle^2 = \left(\frac{\hbar}{2m\omega_{\alpha}} \right) n_{\alpha} \left| \frac{\partial\phi(1)}{\partial r} - \frac{\partial\phi(2)}{\partial r} \right|^2 \quad (3)$$

n_{α} being the phonon occupation number of the α^{th} mode. From the HLO treatment of energy transfer mediated by localized phonons, the probability for one- and two-phonon absorption can be deduced as:

$$\begin{aligned} W_{2 \leftarrow 1}^{-} &= \frac{2\pi}{\hbar} J^2 (f - g)^2 \sum_{\alpha} \frac{|\langle n_{\alpha} - 1 | \Delta\varepsilon | n_{\alpha} \rangle|^2}{(\Delta E_{12})^2} \delta(\Delta E_{12} - \hbar\omega_{\alpha}) \\ W_{2 \leftarrow 1}^{-} &= \frac{2\pi}{\hbar} J^2 (f - g)^4 \sum_{\alpha\beta} \frac{|\langle n_{\alpha} - 1 | \Delta\varepsilon | n_{\alpha} \rangle|^2 |\langle n_{\beta} - 1 | \Delta\varepsilon | n_{\beta} \rangle|^2}{(\hbar\omega_{\alpha})^2 (\hbar\omega_{\beta})^2} \delta(\Delta E_{12} - \hbar\omega_{\alpha} - \hbar\omega_{\beta}) \end{aligned} \quad (4)$$

where $\Delta\varepsilon = \varepsilon(1) - \varepsilon(2)$, \mathbf{J} is the interionic coupling matrix, and f and g are the electron-phonon coupling to excited state, and ground state, respectively.

Two models that describe extreme phonon localization are the fracton model and the 'Einstein modes'. The latter sets ξ to be constant and smaller than the average interatomic spacing. Each atom becomes an independent oscillator[5]. The density of states in this model varies smoothly through the mobility edge, which rules out the possibility of sharp changes in density of states as a reason for any spectral structure formed.

In this investigation weak localization of phonons is assumed with $\xi \cong k^{-1}$ (wavelength of Debye phonon at ω_{mc}). Processes represented by W^+ and W^- become broadly resonant for phonons near ω_{mc} . For rare earth ions with the electron-phonon coupling constants of the 10^2 - 10^3cm^{-1} such probabilities are significantly large to produce structure in the fluorescence spectra [5].

To justify the greater effectiveness of energy transfer mediated by a localized phonon over a Debye phonon with the same energy $\hbar\omega_\alpha$, the gradient of strain for the two is compared. Equation (2), (3), and (4) show the importance of strain gradient in energy transfer. A Debye phonon with energy $\hbar\omega_\alpha$ and wavelength of the order of 10 interatomic spacing, has its elastic strain distributed over a large volume of the medium, while a localized phonon of the same energy extending over a few interatomic separation has the elastic strain distributed over that small number of atoms. A microscopically inhomogeneous system like glass will have regions where strain and its gradient will be considerably greater than for the extended phonons.

For instance [5], a 20cm^{-1} weakly localized phonon with $\xi \approx 8\text{nm}$ has a greater strain gradient than a Debye phonon of the same energy extending over a volume of 600nm in diameter. It has been shown by Dixon, Gang, and Powell[15] that for $\Delta E_{12} = 20\text{cm}^{-1}$, there exists at least one phonon on an average within an interval of 7nm that participates in energy transfer along with many Debye phonons. Yet, the effectiveness of energy transfer due to the localized mode is greater. This is because the vibrations from the single localized phonon are coherent rather than those from the many Debye modes that are incoherent. In the 1cm^{-1} linewidth, the effectiveness of localized phonon in mediating energy transfer is 10^3 times greater than due to Debye phonons.

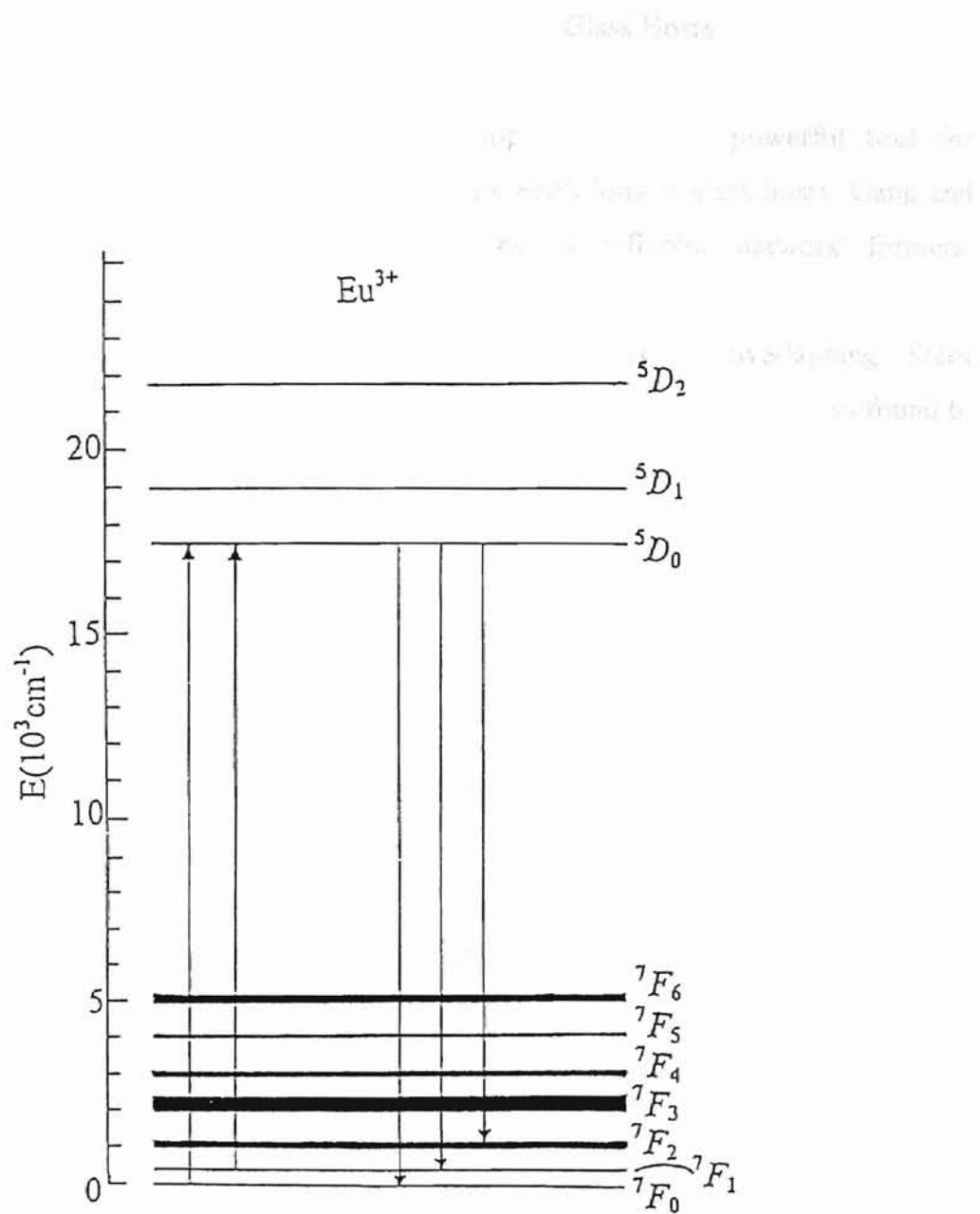


Figure 1.(h) F and D energy levels of Eu³⁺ ions. The widths of the levels indicate the Stark splitting of the crystal field states in glass hosts.

Fluorescence Spectra of Eu^{3+} in Glass Hosts

Site-selection time-resolved spectroscopy has been a powerful tool for probing the spectral structure displayed by rare earth ions in glass hosts. Gang and Powell [3] performed experiments on glasses of different network formers, modifiers, their different chemical compositions and different mol% of the dopant Eu_2O_3 . To avoid ambiguity arising from transitions to overlapping Stark components, the forbidden transition between the singlet states 5D_0 - 7F_0 was found to be most useful in such a study. Energy levels and transitions are shown in fig. 1(h). A tunable dye laser was employed as the excitation source. Excitation transition 7F_0 - 5D_0 followed by its radiative decay 5D_0 - 7F_0 was monitored. The fluorescence spectra observed as time evolved after the excitation pulse showed distinct structure due to energy transfer.

The evolution of spectral profile from smooth band with some structure at early times after laser pulse to a series of distinct peaks at later times is explained as follows. The former structure is due to site-to-site variation of local crystal fields brought about by topological disorder in glasses, that overlap to form an inhomogeneous continuum. On the other hand, the distinct peaks indicate a certain degree of local order in the glass structure, that results in a fewer number of crystal fields, decreasing the overlapping of homogeneously broadened spectral lines and giving rise to discrete resolvable lines.

From their time-resolved spectral observations Gang and Powell concluded that energy transfer occurs to spectrally dissimilar ions throughout the inhomogeneously broadened band. The basis of this conclusion, was attributed to temperature dependence of energy transfer rate associated with thermally populating new levels providing new energy transfer transitions.

Similar site-selective time resolved experiments conducted by Gang, Boulon and Powell[2] to observe spectral transitions of Eu^{3+} in germinate glass host of composition 66 GeO_2 , 17 K_2O , 17 BaO in mol % modified with 1 wt. % Eu^{3+} showed structured fluorescence spectra that evolved into sharper secondary peaks with time,

after laser pulse. From the spectral analysis it was concluded that the discreteness in structure at later times resulted from energy transfer to ions in specific types of sites; site A located at 577.2nm, site B at 578.5nm and site C at 579.5nm. It was observed for this glass host, that energy was transferred from site C at low energy to site A at a higher energy without involving the site B of intermediate energy. Thus participation of thermal vibrations becomes a necessity in the energy transfer process.

Subject of Investigation

Transition probabilities, proportional to the square of an interaction, are potentially sensitive to site-dependent variations in interaction strength than energy levels. In this study, silicate glasses modified with alkaline earth, alkali and 5 mol % Europium ions, serve as the microscopically inhomogeneous medium where disorder in structure makes all sites different from one another. Subject to FLN time-resolved techniques, the ${}^7F_0-{}^5D_0$ transition in Eu ions result in a well structured fluorescence spectra due to energy transfer among different types of sites in the glass host. Electron-phonon coupling responsible for the de-excitation transition with localized phonons as the carriers of energy, is studied. An attempt is made to establish whether the structured spectral profile that results from energy transfer represents correlations in the local energy splitting of the rare earth elements, as suggested by Gang and Powell and Gang, Boulon and Powell, or is due to spectral structure in the phonons, as suggested by Dixon [5].

CHAPTER II

EXPERIMENTAL PROCEDURE

Samples

For this study, samples of silicate glasses with Eu^{3+} doping were investigated. They had the composition 65SiO_2 , $15\text{Na}_2\text{O}$, 15MO , $5\text{Eu}_2\text{O}_3$ where $M = \text{Mg, Ca, Sr, Zn}$ in mol%. The samples were provided by Richard C. Powell. Each sample was cut into a piece of approximately $0.3\text{cm} \times 0.3\text{cm} \times 2\text{cm}$. One end and a side of the parallelepiped were polished to minimize scattering of the laser beam and of the fluorescence produced as the laser passes through the glass. The absorption spectra were obtained on a Cary05 spectrophotometer. Excitation source was a 50W xenophoto lamp.

Experimental Setup

Figure 2(a) shows the schematic layout of the experiment. A tunable dye laser consisting of Continuum Nd:Yag pulse laser and rhodamine 6G dye, served as the excitation source. The pulse duration of the laser was 5ns. The laser operation was chosen to be at 532nm. A set of dichroic mirrors separate and pass the 1064nm fundamental beam to a beam dump, which assures a safe disposal of all unused beams. The second harmonic beam was directed into an attenuator with the help of two coated mirrors. The attenuator reduced the power of the laser beam from 3.2W to 70mW. The resulting beam was made to enter DL II Dye Cell Chamber. This pump beam is further weakened in intensity by a 20-25% beam splitter. The DL II dye laser has two cuvette dye cells, both of which are filled with 2ml of rhodamine 6G, their concentrations being 144mg/100cc of ethanol for the oscillator cuvette and 80mg/100cc of ethanol for the amplifier cuvette. Tuning of the pump beam to lower its energy is done by the oscillator

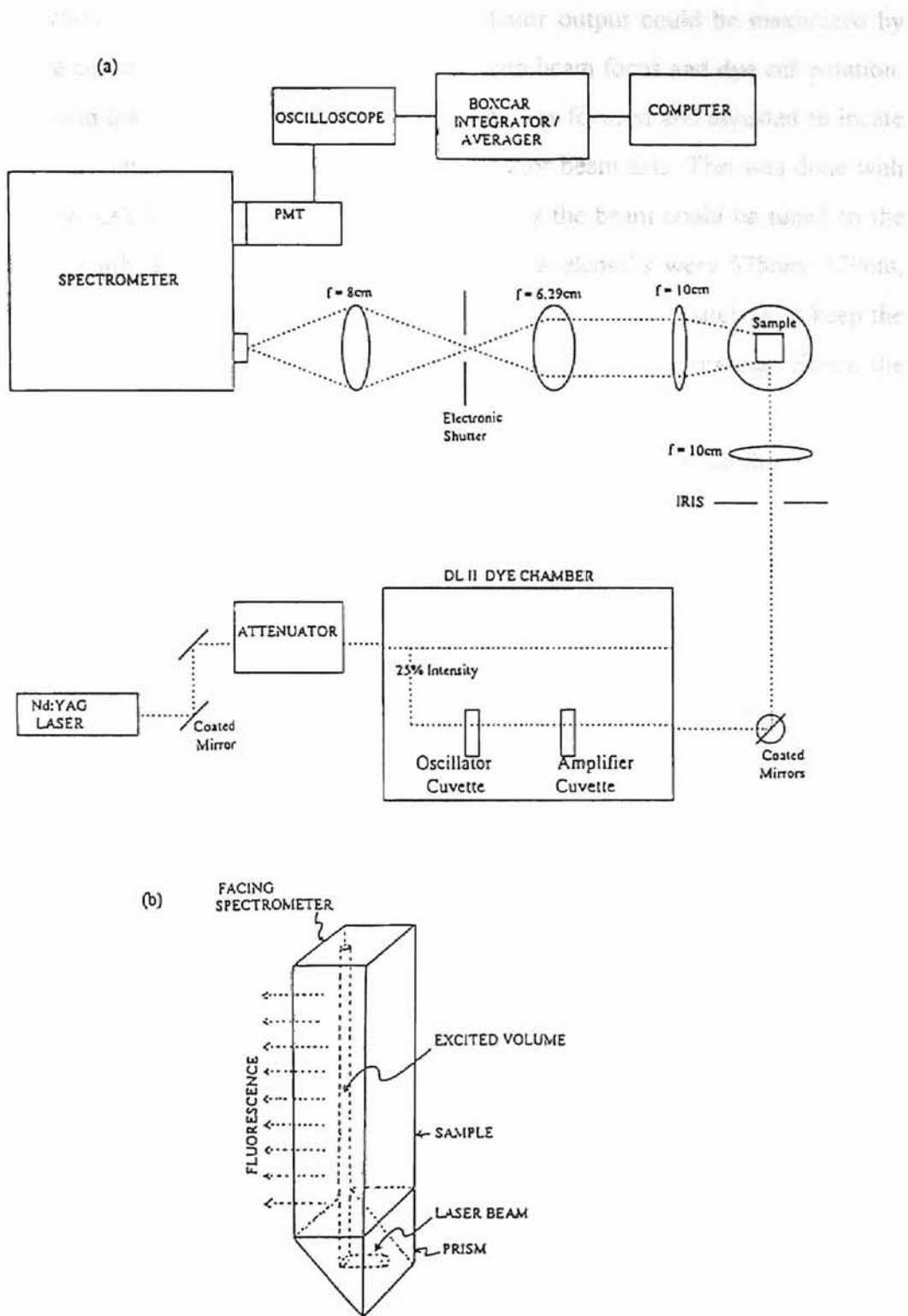


Figure 2. (a) Experimental setup to study energy transfer. (b) The prism reflects the laser beam through the glass sample producing a vertical fluorescent column in it.

with the oscillator cuvette installed in it. The oscillator output could be maximized by adjusting dye cell translation, pump beam height, pump beam focus and dye cell rotation. The pump beam that emerges from the oscillator axis was focused and adjusted to locate the excited-dye volume of the amplifier, on the oscillator beam axis. This was done with the help of dye cell height and translation control. Thus the beam could be tuned to the desired wavelength. For this investigation the tuned wavelengths were 578nm, 579nm, 580nm. The power of the incoming beam into the dye laser should be such as to keep the organic dye from being damaged and to keep the cuvette from cavitating. Hence the reason to attenuate the pump beam to ~70mW.

The tuned beam was reflected off of a pair of mirrors and directed through an iris 1cm. in diameter (to minimize scattered light from the beam), followed by a lens of focal length 10cm.

The sample was mounted in the cryostat as shown in figure 2(b). The focused beam was reflected by a right angle prism into the sample along its long axis. The energy of the incoming radiation was absorbed by Eu^{3+} ions along its path. This was followed by radiative de-excitation of Eu^{3+} ions, visible as a column of fluorescence along the axis of the sample.

The excited volume was situated at the focus of a convex lens with focal length of 10cm. The parallel rays that emerged from the lens formed an image at the focus of a convex lens of focal length 6.29cm. This image was 2/5 times the original object. It was brighter and sharper, as well. An electronic shutter with an aperture comparable to the size of this line shaped image let the fluorescence pass through, which was refocused at the shutter of a 0.85m monochromator. The fluorescence had both, the intense excitation and the relatively weaker de-excitation radiation, the subject of interest. To minimize the former and maximize the latter, the exposure time and the delay time before the electronic shutter reopens, was optimized.

Spectrometer

The image of the fluorescent line after passing through the aperture of the electronic shutter appeared as a fluorescent dot that approximately filled the width of the

2cm. X 0.5cm. entrance of the spectrometer. The slit width was then narrowed to 100 μ m to eliminate the scattered light from the laser. The slits in the middle were left open. The slit at the exit to the photomultiplier tube(PMT) was set at 100 μ m. The PMT detected the fluorescence analyzed by the spectrometer. The PMT operation was controlled by SPEX 286 computer software, viz., SPEX DM3000S, and the DM303M input module from the integrator unit.

Processing Units

The PMT was connected to an oscilloscope that displayed the detected signal in mV. The signal was sent through a Gated Integrator (Model 4422) followed by a Boxcar Averager (Model 4420). This was to reduce the signal to noise ratio by a factor of 10. To observe the signal and its behavior at specific times after the excitation pulse, it was sent through a signal processor (Model 4402).

Processed by the above three units the improved signal was sent to the computer by DM303M output module. As the data were being taken by the computer, the spectral development could be observed on the monitor.

The sample was mounted as is shown in figure 2(b) in a cold finger connected to a cryogenic refrigerator system, turbo molecular diffusion pump attached to a pressure monitor and a temperature controller connected to the temperature monitor cum heater. The dewar was rough pumped to about 10 μ Torr. Then the turbo molecular pump reduced it to $\sim 10^{-7}$ Torr. The compressor was then switched on. When the temperature dropped to 250K the heater, preset to 70K was switched on.

Scan Specifications

The dye laser was tuned to three excitation wavelengths (λ_{ex}), 578nm, 579nm and 580nm, respectively. The tunable laser tuned to a particular λ_{ex} was scanned across a region between 577.5nm and 580.5nm. For each scan the fluorescence was observed after 1ms, 3ms, 5ms, 7ms, and 9ms, respectively after the resonance excitation. Fluorescence

was observed through a gate $298\mu\text{s}$ wide. The 'exposure time' on the electronic shutter and the 'delay time' after which the shutter reopens were 32ms and 14.1ms, respectively. The scan plot by the computer is set to show wavelength in nanometers on the X-axis and intensity in volts on the Y-axis. Integrated and averaged value of intensity was obtained at the end of a 10s interval for a wavelength increment of 0.02nm. The resulting scan had duration of 25min. Observations were made at a preset temperature of 70K.

CHAPTER III

RESULTS AND DISCUSSIONS

A Eu^{3+} ion has a simple energy level scheme as compared to other lanthanide ions such as Yb^{3+} , Nd^{3+} , Mo^{3+} , etc. Therefore Eu^{3+} incorporated into various glasses form an interesting subject to various spectroscopic investigations. Gang, Boulon and Powell and Gang and Powell [2,3] studied the time evolution of laser induced resonant line-narrowed spectrum in Eu^{3+} . As a specific case, the transition studied was ${}^5D_0 \rightarrow {}^7F_0$, forbidden by the electric dipole transition selection rules, in glasses.

Typically, a time evolution process of the fluorescence is as follows. Following the laser pulse, the initial line narrowed fluorescence decays by a combination of radiative and non-radiative energy transfer to other Eu^{3+} ions without significant line broadening. Subsequently the process is repeated by the acceptor ions, and a new inhomogeneously broadened equilibrium emission profile is formed indicating energy transfer to the neighboring dissimilar sites. This energy transfer is not to the central resonant site only, but to all the sites within the inhomogeneous profile. This process is attributed to polar processes and is associated to crystal fields that vary from one type of site to another [1].

Gang and Powell [3] selectively excited sites on the high and the low energy sides of the absorption band for seven samples. The glass samples varied in chemical composition, network formers, network modifiers, their mol %, and the Eu^{3+} ion concentration. Fluorescence spectra obtained at two times after laser excitation showed marked spectral evolution due to energy transfer. The narrowed line excitation decreased as the inhomogeneous profile increased and became more discrete in structure with time. At very long times after the laser pulse, the spectral profile approached the inhomogeneous band profile. The observed structure can be explained as being caused by ligand field sites that are different from one another. When only a few of the many

ligand field sites are excited by energy transfer, the resulting homogeneously broadened spectral lines do not overlap, but form a series of distinct resolvable lines.

In this investigation, the experiment performed with four glass samples of composition described in chapter II using the experimental set up shown in fig 2(a), yielded time resolved spectra as displayed in fig 3-14. Normalizing these spectra with respect to the absorption band spectra of each of the samples (fig 15-18), fig 19-30 are obtained. Graphs generated by calculating the ratio of intensities make the time resolved spectra clearly observable. Series of distinct peaks developing into more resolvable lines can be seen, for the reason that energy is being transferred from one type of site to another. This can be attributed to either correlation effect due to the structure of glass or due to localized phonons mediating the energy transfer.

Energy Transfer Function $a(t)$

Time resolution of the emission spectra of Eu^{3+} ions in various glasses show structure that indicates energy transfer to ions in different types of sites with a possible involvement of a mechanism. A method developed by Brawer and Weber quantitatively characterizes energy transfer [8]. Time evolution of the normalized spectral profile can be expressed as

$$I(\omega, t) = a(t)I(\omega, 0) + [1 - a(t)]I(\omega, \infty) \quad (4)$$

where $a(t)$ is the function that describes the energy transfer with time. Rearranging (4) to calculate $a(t)$ gives

$$a(t) = \frac{\int_{\omega_1}^{\omega_2} [I(\omega, t) - I(\omega, \infty)] d\omega}{\int_{\omega_1}^{\omega_2} [I(\omega, 0) - I(\omega, \infty)] d\omega} \quad (5).$$

ω_1 and ω_2 define the limits of the region of excitation and $a(t)$ represents the migration of energy from the central resonantly excited ions to other types of sites in the inhomogeneous band.

In this investigation, spectra were obtained after time delay of 1ms, 3ms, 5ms, 7ms, and 9ms after the laser excitation. Substituting $t=1\text{ms}$ for $t=0$ in (5) for the initial time, assuming that at $t \rightarrow \infty$ the fluorescence intensity approaches that of the broad band absorption, and adjusting the baseline so as to be able to neglect the normalized intensity I as $t \rightarrow \infty$, (5) can be approximated as :

$$a(t) \cong \frac{\sum_{\lambda_{ex}-0.5\text{nm}}^{\lambda_{ex}+0.5\text{nm}} \left(\frac{I(t)}{\sum_{577.5\text{nm}}^{580.5\text{nm}} I(t)} \right)}{\sum_{\lambda_{ex}-0.5\text{nm}}^{\lambda_{ex}+0.5\text{nm}} \left(\frac{I(1\text{ms})}{\sum_{577.5\text{nm}}^{580.5\text{nm}} I(1\text{ms})} \right)} \quad (6)$$

$I(\omega, t)$, and $I(\omega, 0)$ in (5) now become :

$$I(\omega, t) \approx \left(I(t) / \sum_{577.5\text{nm}}^{580.5\text{nm}} I(t) \right)$$

$$I(\omega, 0) \approx \left(I(1\text{ms}) / \sum_{577.5\text{nm}}^{580.5\text{nm}} I(1\text{ms}) \right)$$

and $I(\omega, \infty) \approx$ negligible.

Fig.(32-35) of energy transfer function versus time delay after excitation pulse, show $a(t)$ as an exponentially decaying function of time, as energy is transferred from the central resonant ions to the ions of different types of sites, with varying values of α , the characteristic decay time. Gang and Powell [3] on the basis of their analysis on different glasses argued that α represents the average value for energy transfer time to ions in all sites spread throughout the inhomogeneous band. Therefore the calculated value of α could not be directly related to any specific type of transfer mechanism. Correspondingly, there is an exponential rise of $a(t)$ for the secondary peaks (fig. 36-37). From the fluorescence spectra (fig. 19-30) it can be observed that there is a region between 578.5 and 579nm where a structure can be seen as growing with time after the laser excitation pulse, indicating an energy transfer into that region. This implies that there are preferential absorption transitions between energy levels in Eu^{3+} ions that

require energy within the above mentioned range. Inhomogeneously broadened absorption band spectra for each sample at room temperature (fig 15-18) show the region of maximum intensity, that includes the interval between 578.5 and 579nm corresponding to a large number of ions that absorb energy in this region. Thus it can be said that there is a distinct set of sites acting as acceptors of energy within this interval; the structure seen in the fluorescence scan for a sample is due to a large number of such ions. This information supports energy transfer due to correlation in the structure of glasses.

However, the structure in fluorescence spectra i.e., the secondary peaks other than the one discussed above appear at varying locations on the energy scale for different samples, subject to different λ_{ex} . Table I compares the wave number at which Raman activity begins for each sample, to those which determine the onset of the secondary spectral structure. Raman activity requires that the wave vector of the energy carrying phonons be changed for conservation of energy. k then is no longer a valid quantum number. This favors the energy carrying phonons to be localized. Thus the frequency at which the localization takes place, in this case, at the onset of the low frequency boson peak is chosen as the frequency at the mobility edge. Phonons with frequencies less than ω_{mc} are not localized. Figure 36 shows $a_1(t)$ for the first peak appearing on the shoulder of the central resonant peak, decreasing with time. The rising edge of the secondary peak begins at 7cm^{-1} at $\lambda_{ex} = 578\text{nm}$ for the Ca-modified glass. Since ω_{mc} corresponds to Raman activity beginning at $14\text{cm}^{-1} > 7\text{cm}^{-1}$, $a_1(t)$ decays with time. Hence an evidence for the effect of localization not observable for phonons with frequencies less than ω_{mc} . Increase in $a(t)$ values for the onset of secondary peaks at frequencies greater than ω_{mc} may indicate that energy transfer is mediated by localized phonons, as their efficiency in transferring energy is far greater than Debye phonons of the same energy.

It is noted that $a(t)$ for the secondary peaks rises to approach a saturated value at large times after the laser pulse, compared to its characteristic time, α (fig 36-37). Similarly the resonantly excited peak falls in its $a(t)$ value until it approaches a constant

value at large times, compared to its characteristic decay time, α , thus indicating that at such large times, energy transfer rate from the central resonant peak to the secondary peaks, and from the latter in turn, to their surrounding acceptor sites and so on, reaches a steady value. Therefore it is possible to observe the time-resolved structure in the fluorescence spectra within only a limited time interval beyond which the multistep transfer will tend to dissipate the structure.

From table I peak-spacing i.e., the frequency interval between the onset of one secondary peak and the next consecutive one can be calculated. Zn-modified glass shows peak spacing in the range from 7 to 10 cm^{-1} ; Mg-modified glass, between 7 and 11 cm^{-1} ; Sr-modified glass, between 7 and 11 cm^{-1} , and Ca-modified glass between 8 and 10 cm^{-1} . Thus it can be said that the secondary peaks are regularly spaced to the uncertainty of $\pm 2\text{cm}^{-1}$ for these glasses. Dixon [5] proposes that the peak-spacing should correspond to the low frequency mobility edge for phonon localization (fig 31). The calculated data in table I agrees with the theory. However, the onset of boson peak is different from the spacing between the peaks; the latter being smaller than the former in the frequency regime for all samples. A possible explanation could be that at the onset of Raman activity both Debye phonons and localized phonons of the same energy may coexist thus partially obscuring the manifestation of phonon localization at a frequency that is a near integral multiple of the peak spacing. Table II shows the frequency values at the onset of the secondary peaks in the frequency regime, with 17316 cm^{-1} (577.5nm) as the reference frequency. The peak spacings are found to have the similar values as those obtained from table I within $\pm 2\text{cm}^{-1}$. The near constant peak spacing independent of laser excitation at any wavelength for all the samples under investigation is suggestive of an energy transfer mediated by localized phonons of frequencies comparable to the secondary peak spacing.

It may be possible to improve the agreement by a more careful deconvolution of the fluorescence from the absorption profile and homogeneous linewidths. This is beyond the scope of the present work.

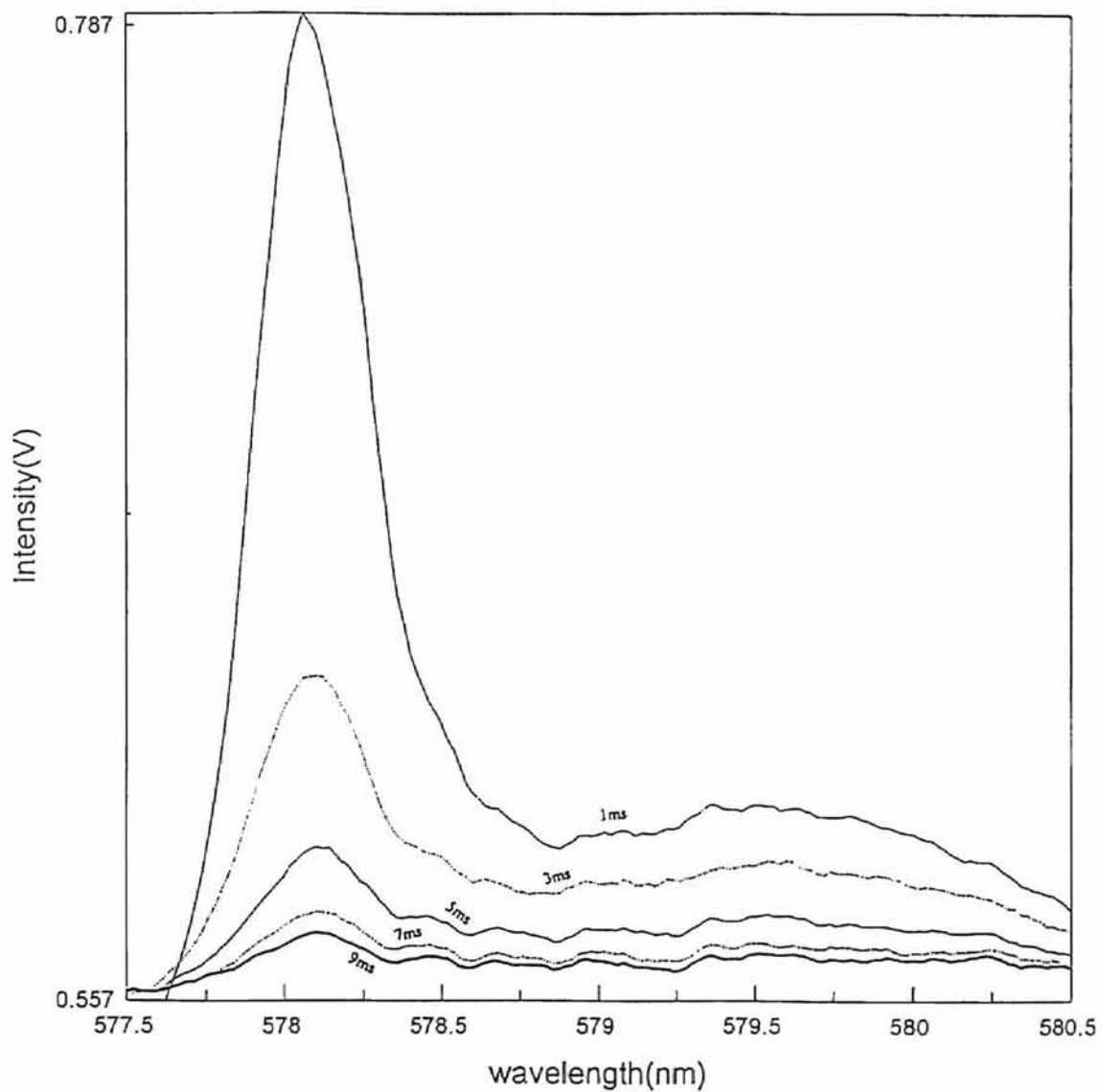


Figure 3. Spectra of Eu^{3+} in Ca-modified glass 1ms, 3ms, 5ms, 7ms, and 9ms after the excitation pulse; $\lambda_{\text{ex}} = 578 \text{ nm}$.

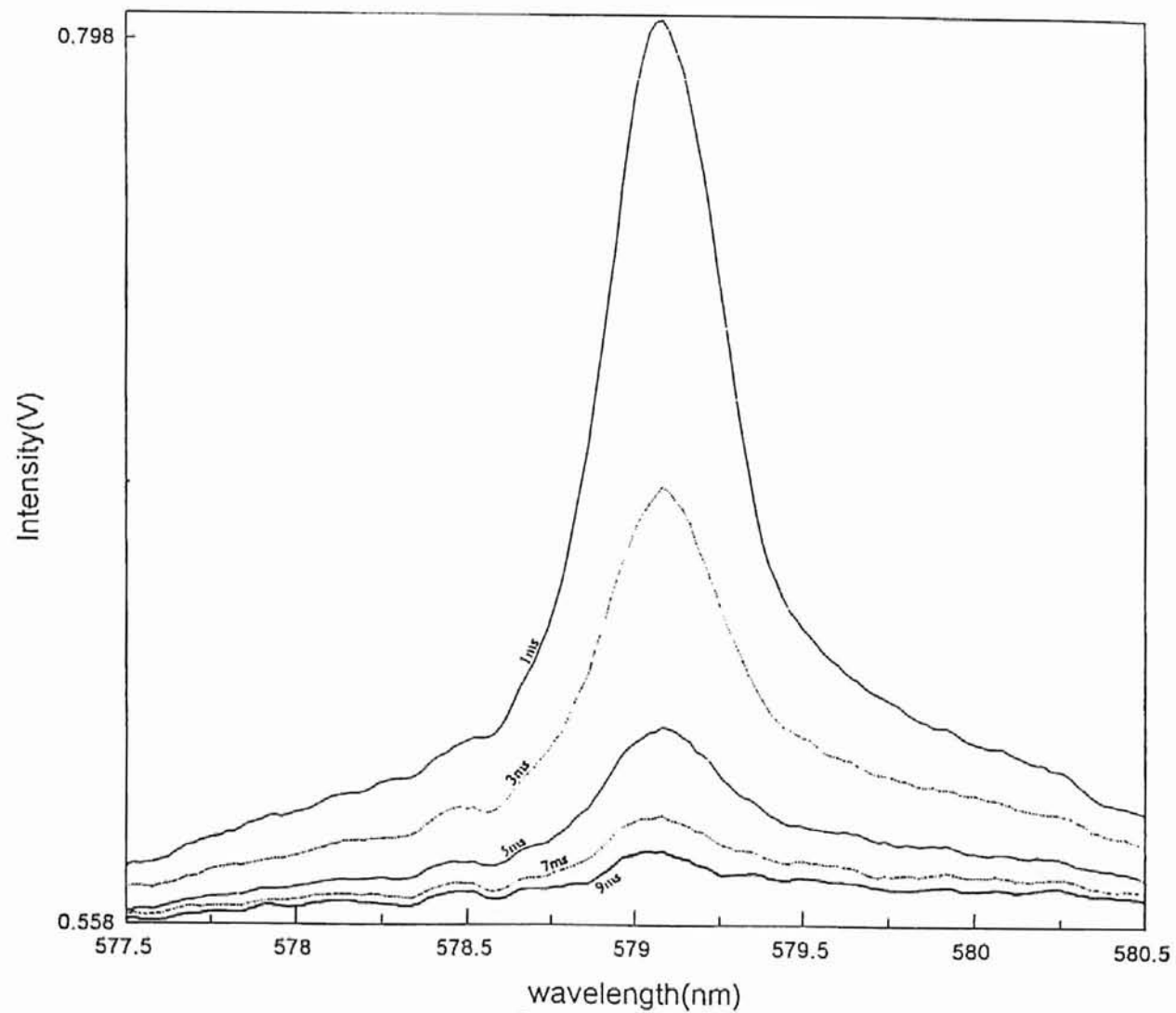


Figure 4. Spectra of Eu^{3+} in Ca-modified glass 1ms, 3ms, 5ms, 7ms, and 9ms after the excitation pulse; $\lambda_{\text{ex}} = 579\text{nm}$.

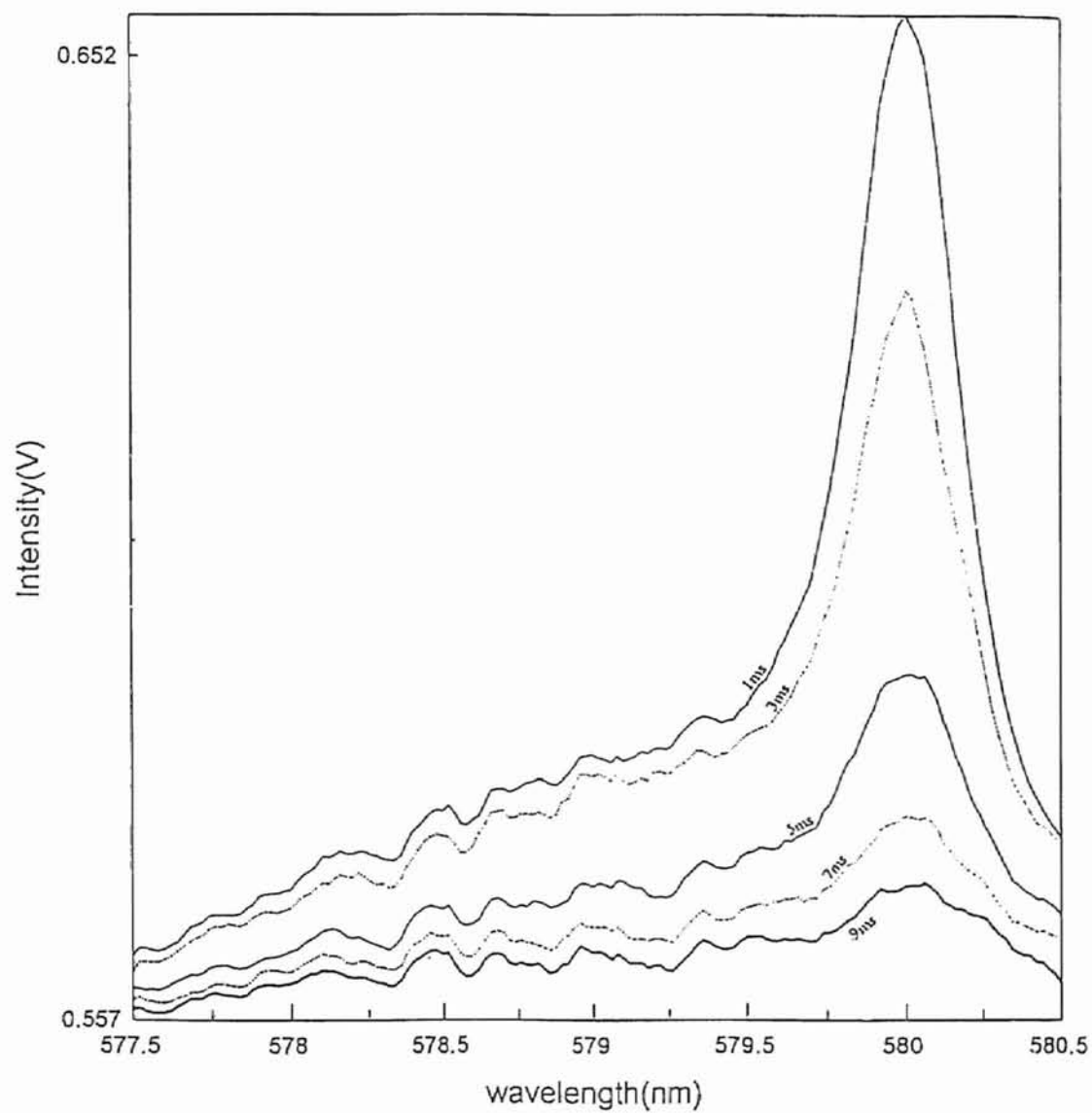


Figure 5. Spectra of Eu^{3+} in Ca-modified glass 1ms, 3ms, 5ms, 7ms, and 9ms after the excitation pulse; $\lambda_{\text{ex}} = 580\text{nm}$.

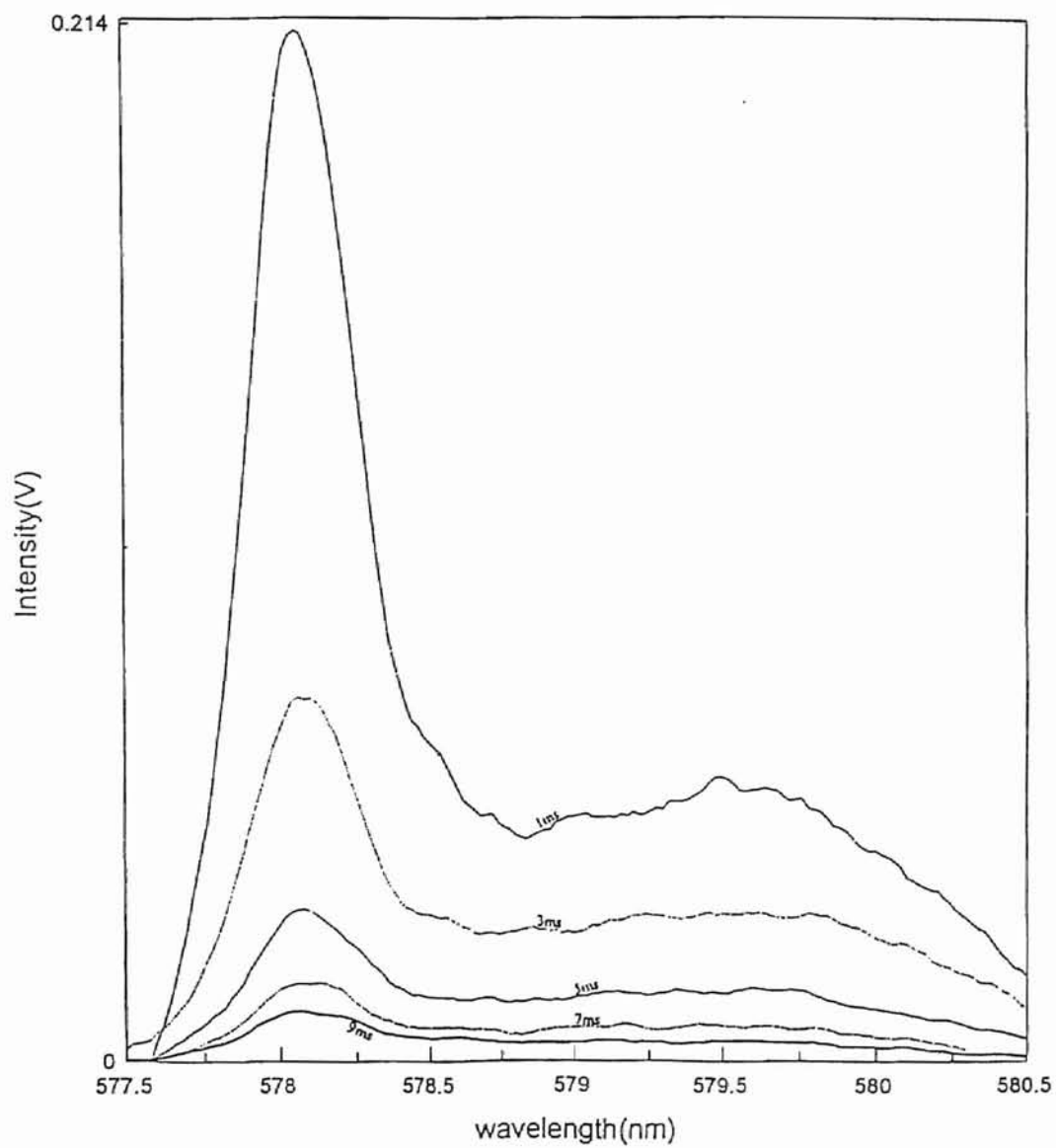


Figure 6. Spectra of Eu^{3+} in Mg-modified glass 1ms, 3ms, 5ms, 7ms, and 9ms after the excitation pulse; $\lambda_{\text{ex}} = 578 \text{ nm}$.

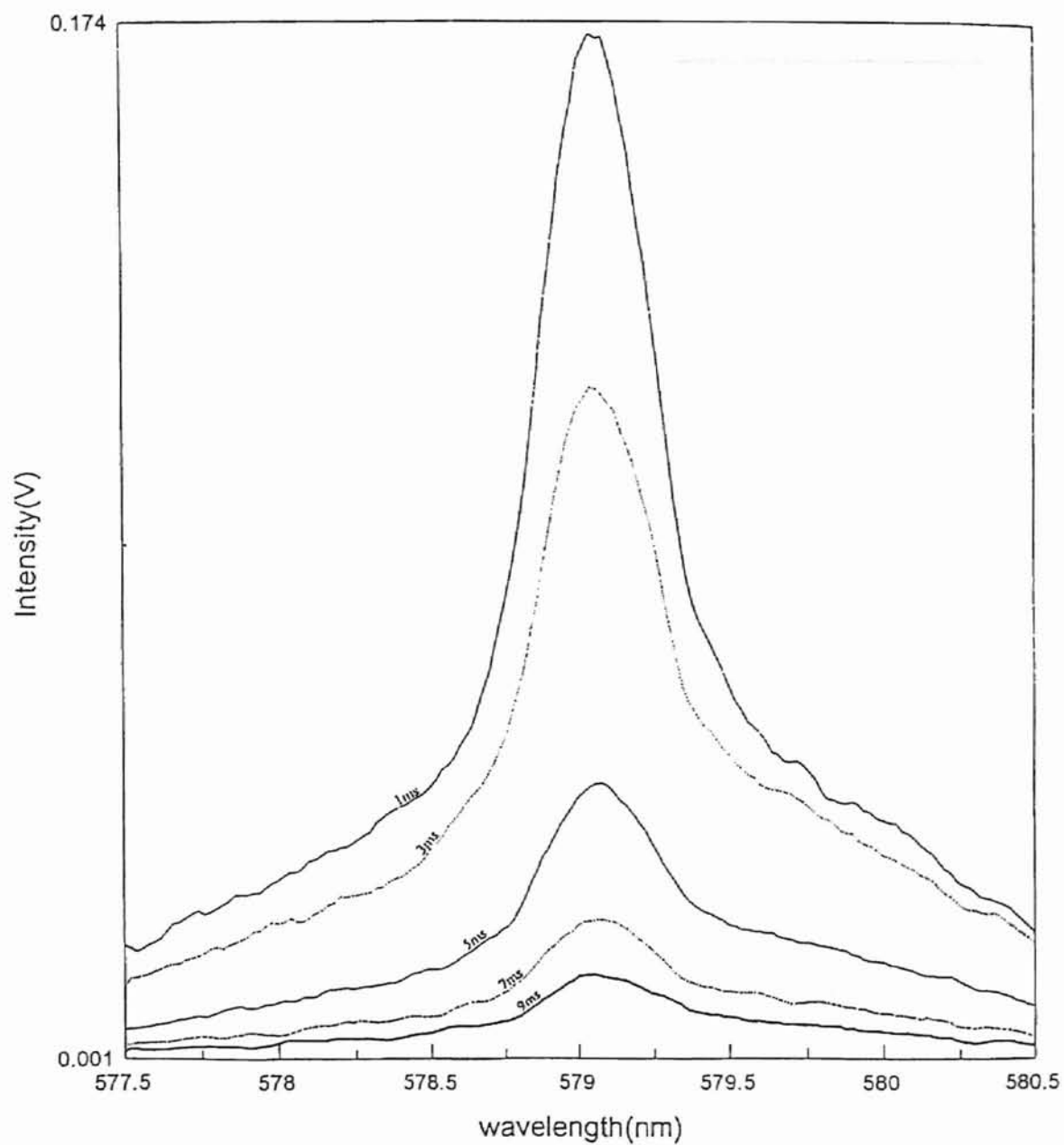


Figure 7. Spectra of Eu^{3+} in Mg-modified glass 1ms, 3ms, 5ms, 7ms, and 9ms after the excitation pulse; $\lambda_{\text{ex}} = 579\text{nm}$.

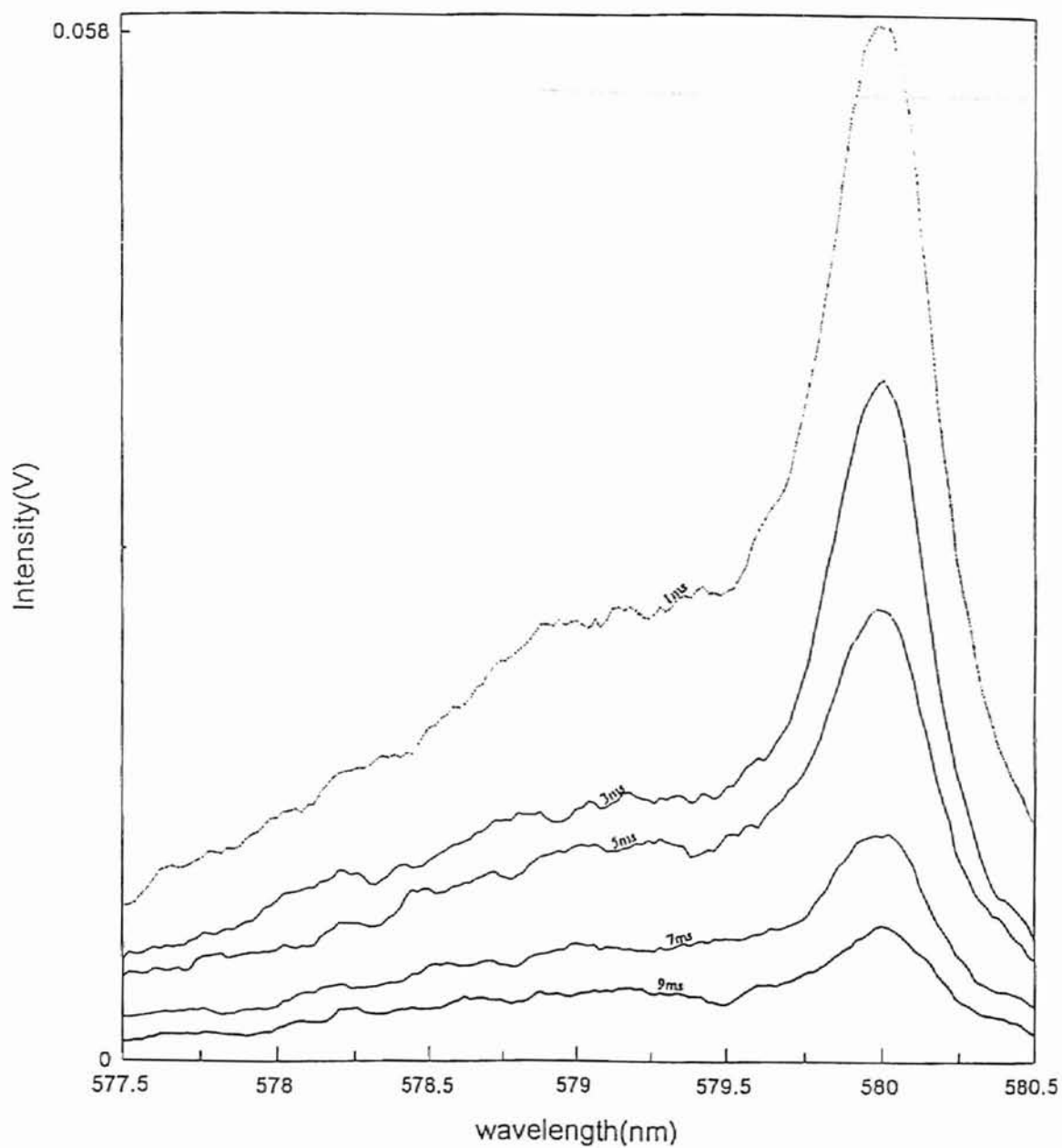


Figure 8. Spectra of Eu^{3+} in Mg-modified glass 1ms, 3ms, 5ms, 7ms, and 9ms after the excitation pulse; $\lambda_{\text{ex}} = 580\text{nm}$.

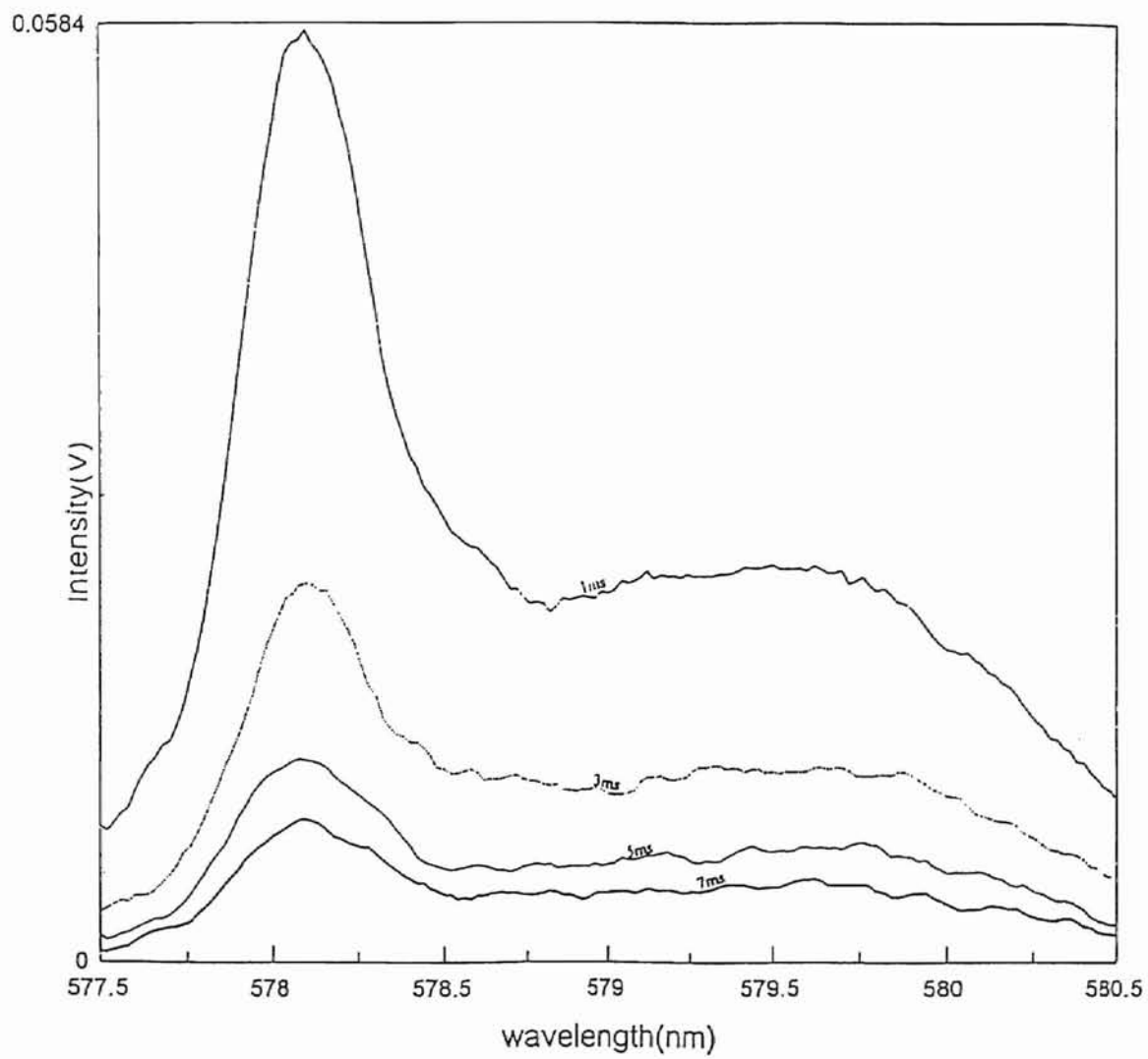


Figure 9. Spectra of Eu^{3+} in Sr-modified glass 1ms, 3ms, 5ms, 7ms, and 9ms after the excitation pulse; $\lambda_{\text{ex}} = 578\text{nm}$.

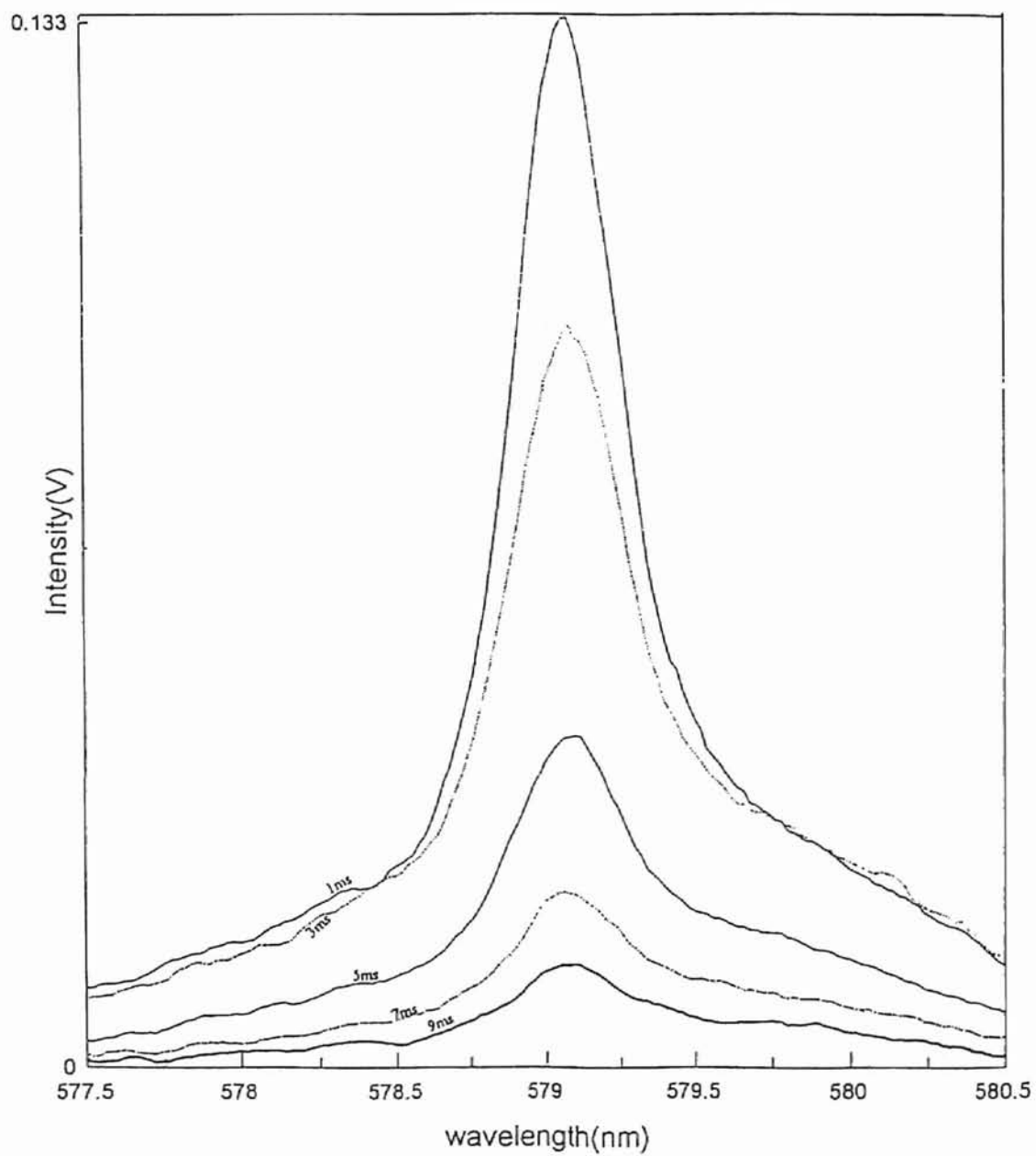


Figure 10. Spectra of Eu^{3+} in Sr-modified glass 1ms, 3ms, 5ms, 7ms, and 9ms after the excitation pulse; $\lambda_{\text{ex}} = 579\text{nm}$.

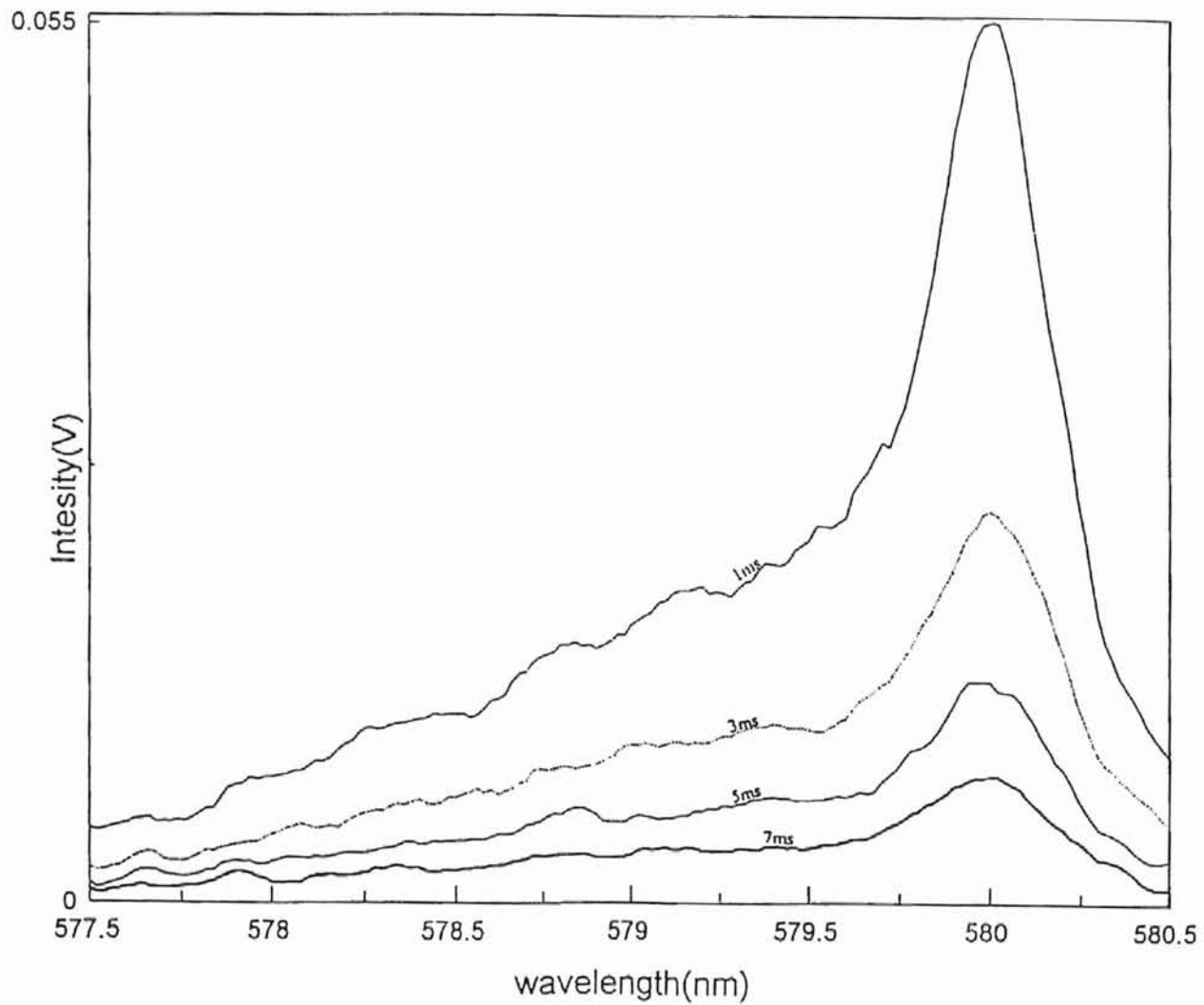


Figure 11. Spectra of Eu^{3+} in Sr-modified glass 1ms, 3ms, 5ms, 7ms, and 9ms after the excitation pulse; $\lambda_{\text{ex}} = 580\text{nm}$.

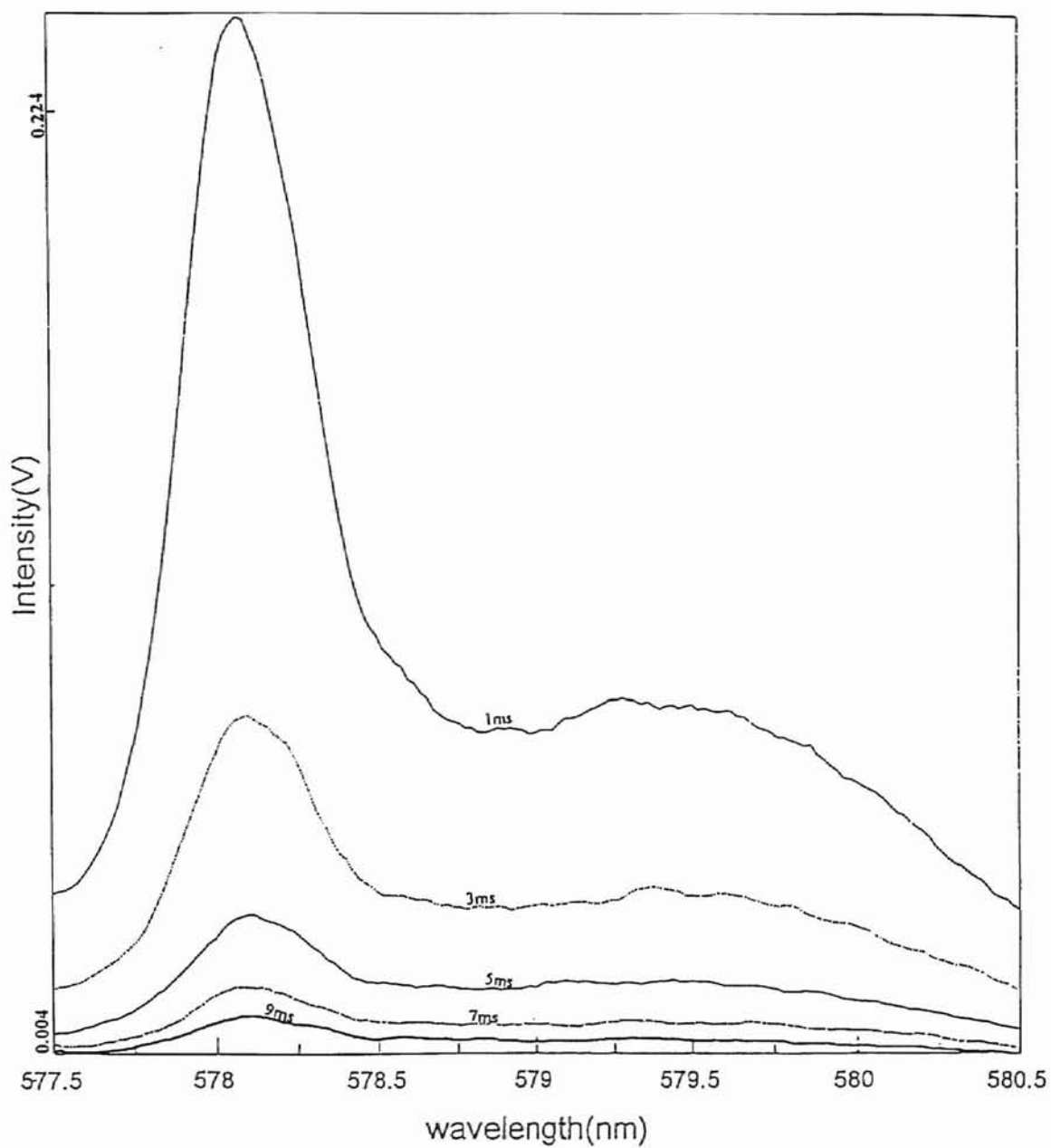


Figure 12. Spectra of Eu^{3+} in Zn-modified glass 1ms, 3ms, 5ms, 7ms, and 9ms after the excitation pulse; $\lambda_{\text{exc}} = 578\text{nm}$.

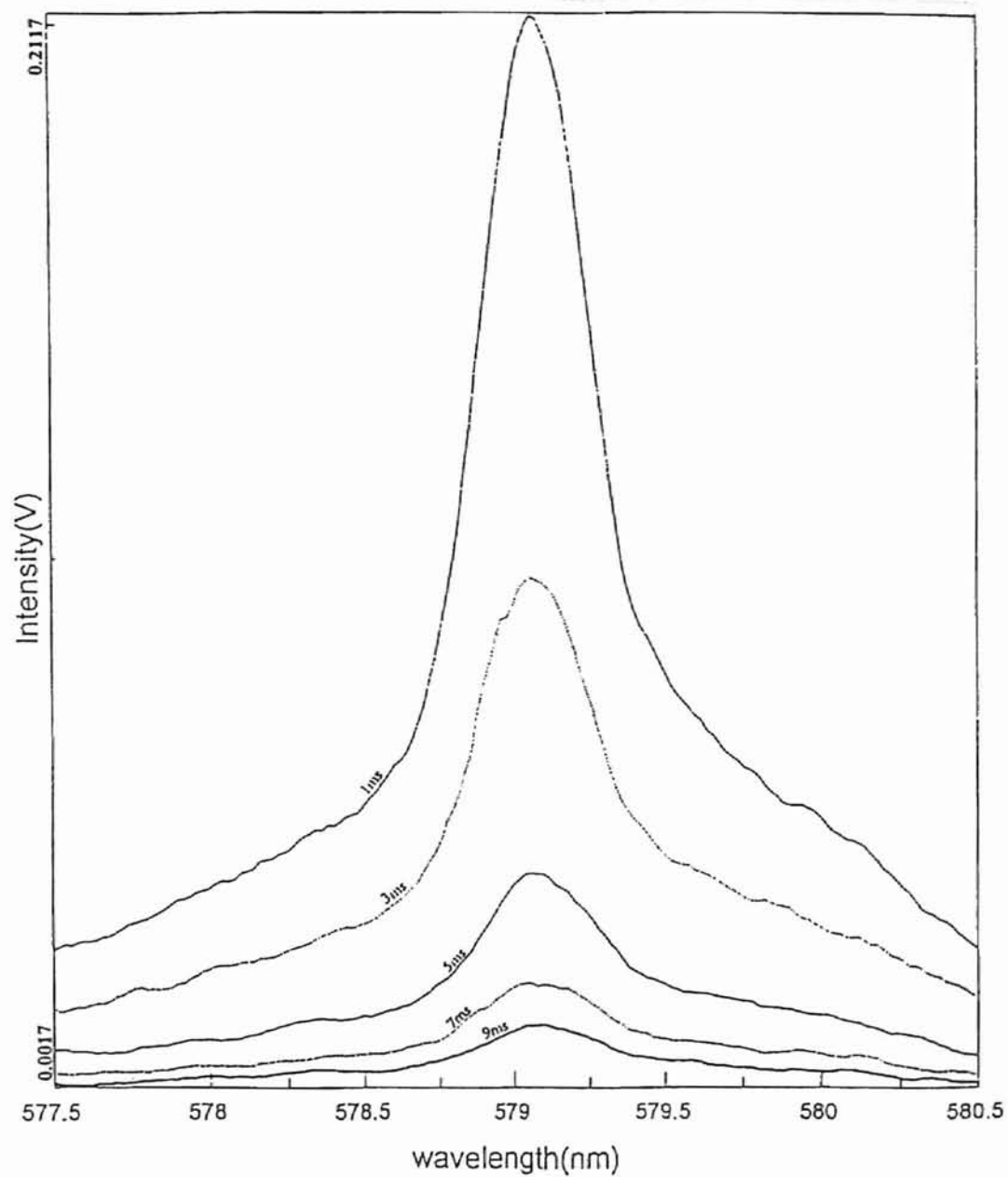


Figure 13. Spectra of Eu^{3+} in Zn-modified glass 1ms, 3ms, 5ms, 7ms, and 9ms after the excitation pulse; $\lambda_{\text{ex}} = 579 \text{ nm}$.

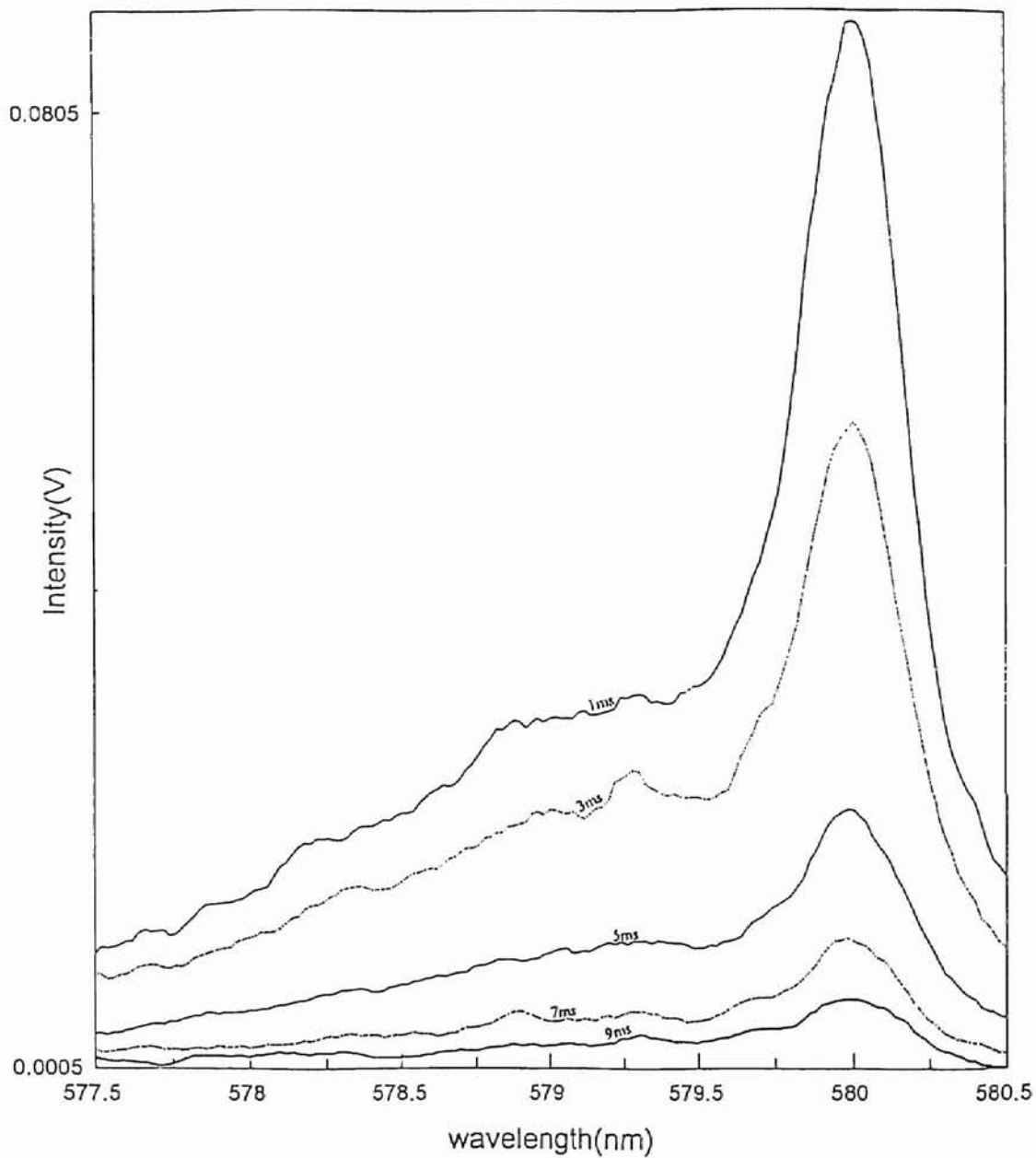


Figure 14. Spectra of Eu^{3+} in Zn-modified glass 1ms, 3ms, 5ms, 7ms, and 9ms after the excitation pulse; $\lambda_{\text{ex}} = 580\text{nm}$.

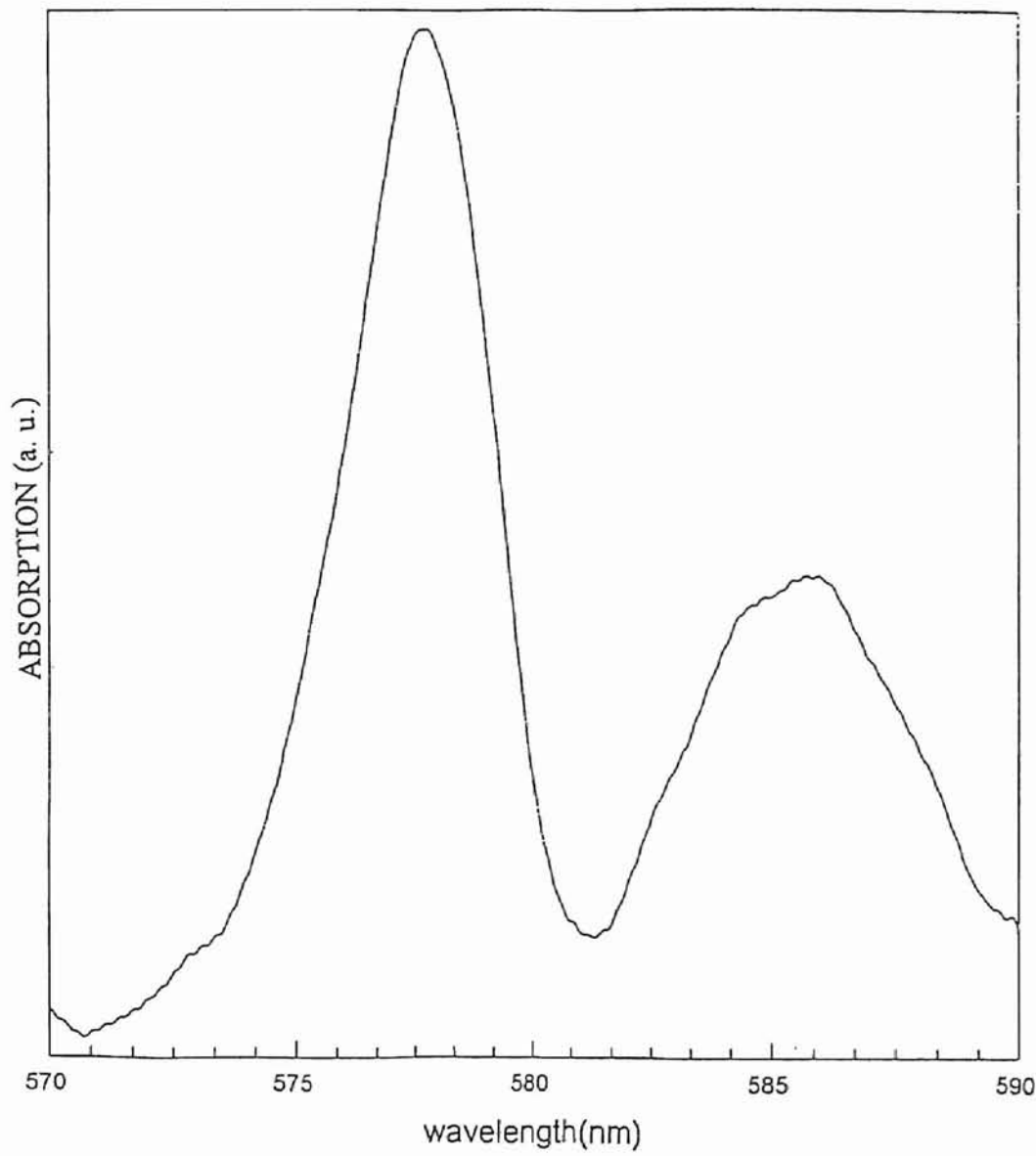


Figure 15. Inhomogeneously broadened absorption band spectra for Ca-modified glass obtained from Cary05 spectrophotometer at room temperature.

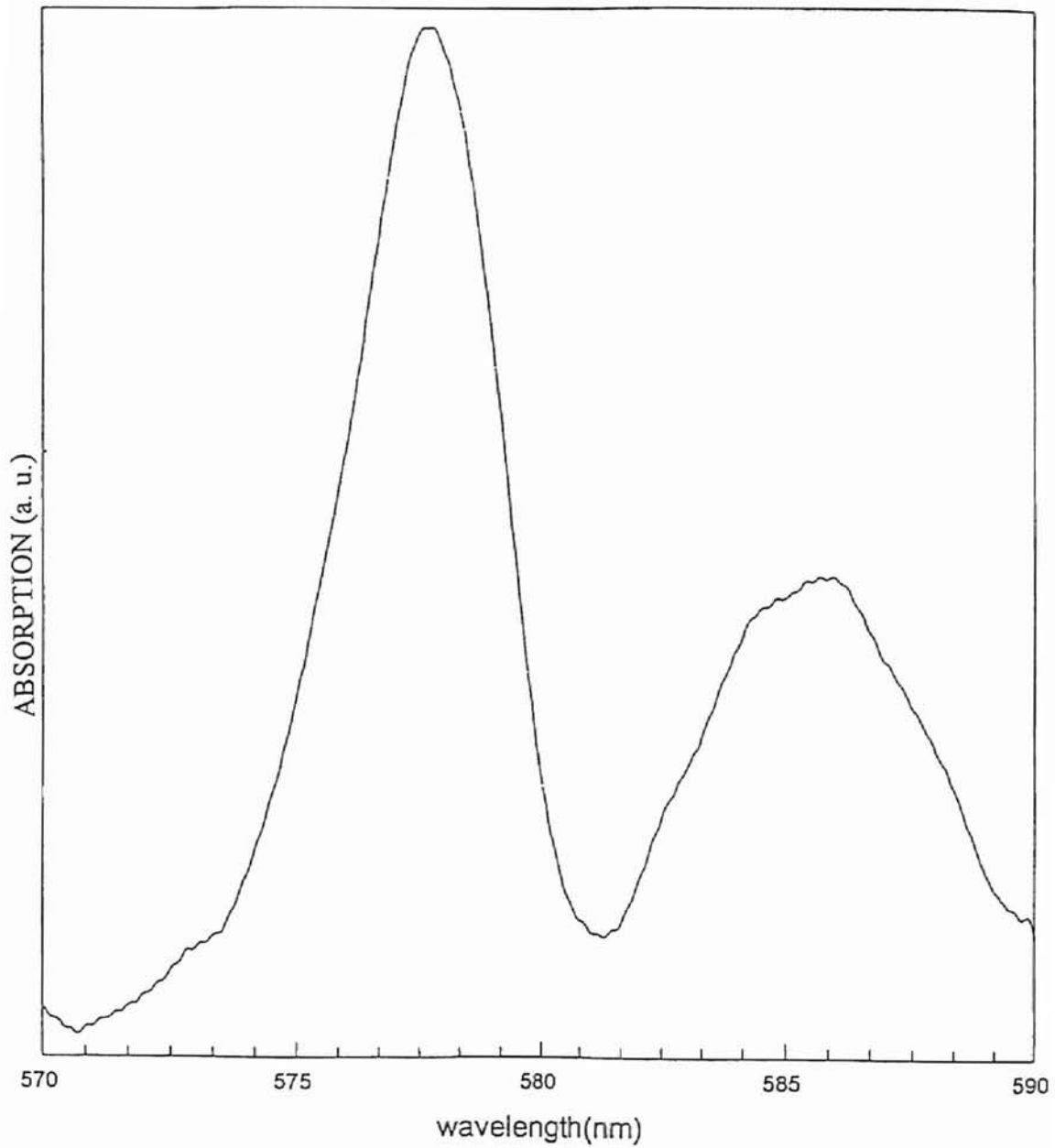


Figure 16. Inhomogeneously broadened absorption band spectra for Mg-modified glass obtained from Cary05 spectrophotometer at room temperature.

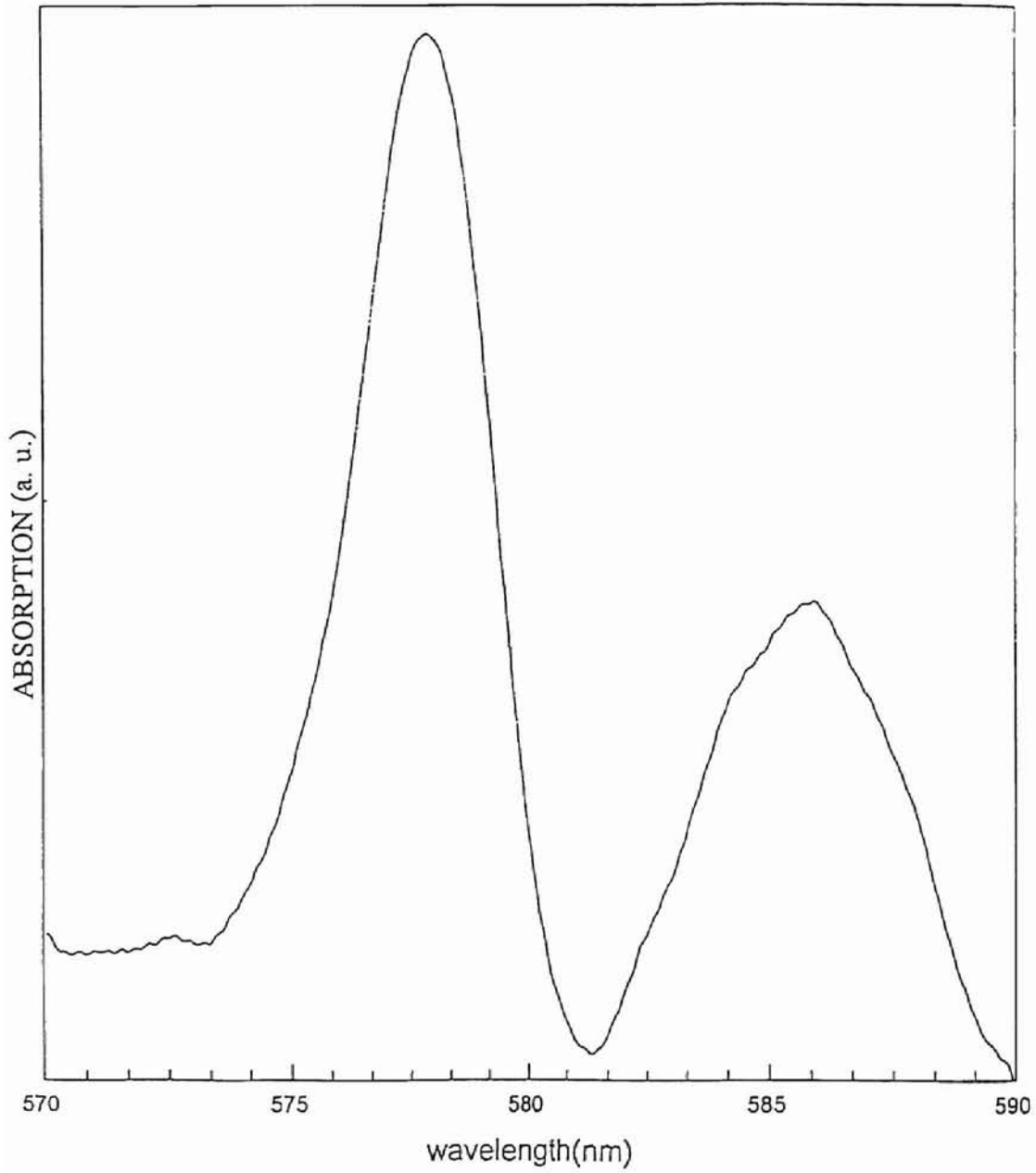


Figure 17. Inhomogeneously broadened absorption band spectra for Sr-modified glass obtained from Cary05 spectrophotometer at room temperature.

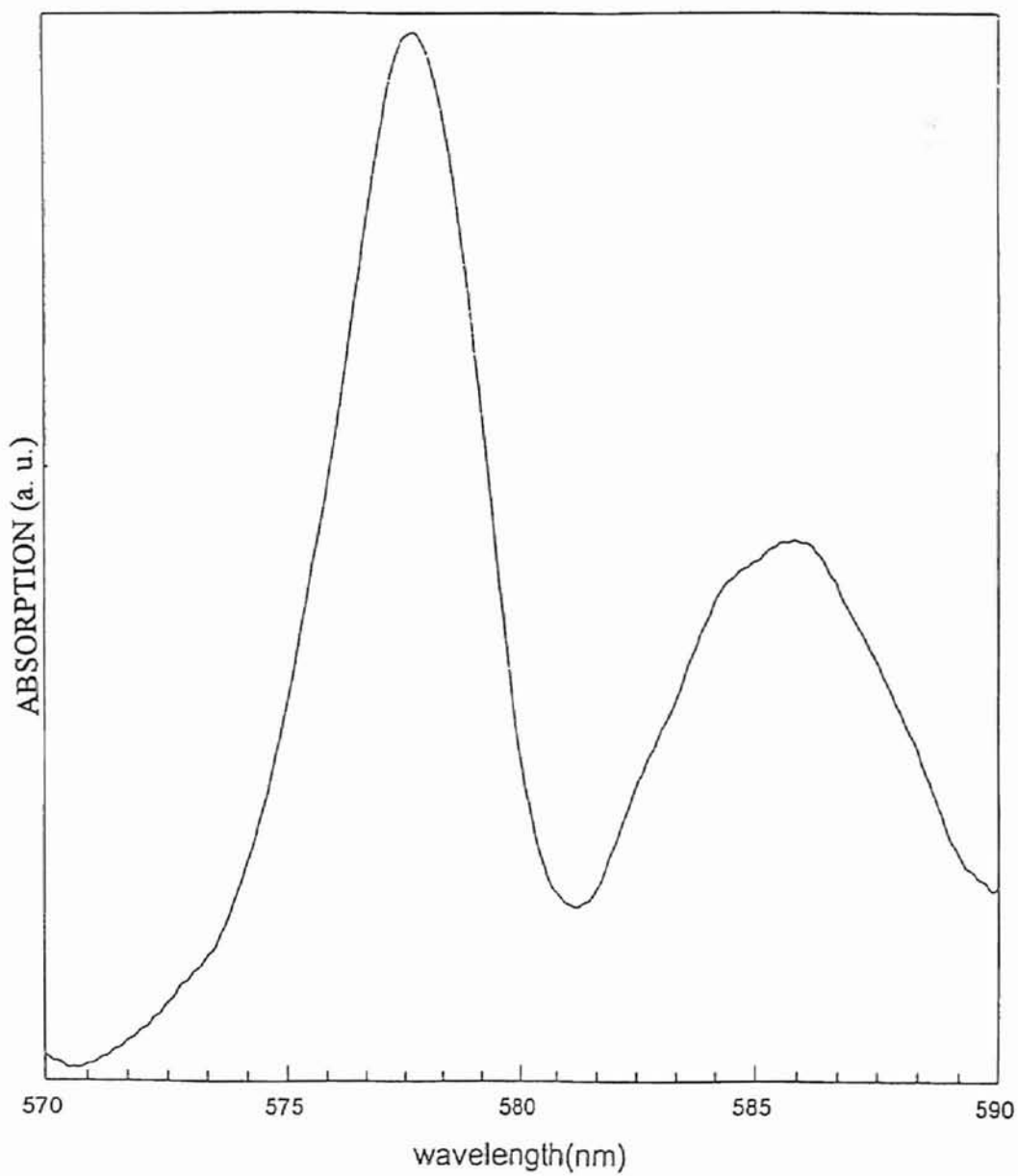


Figure 18. Inhomogeneously broadened absorption band spectra for Zn-modified glass obtained from Cary05 spectrophotometer at room temperature.

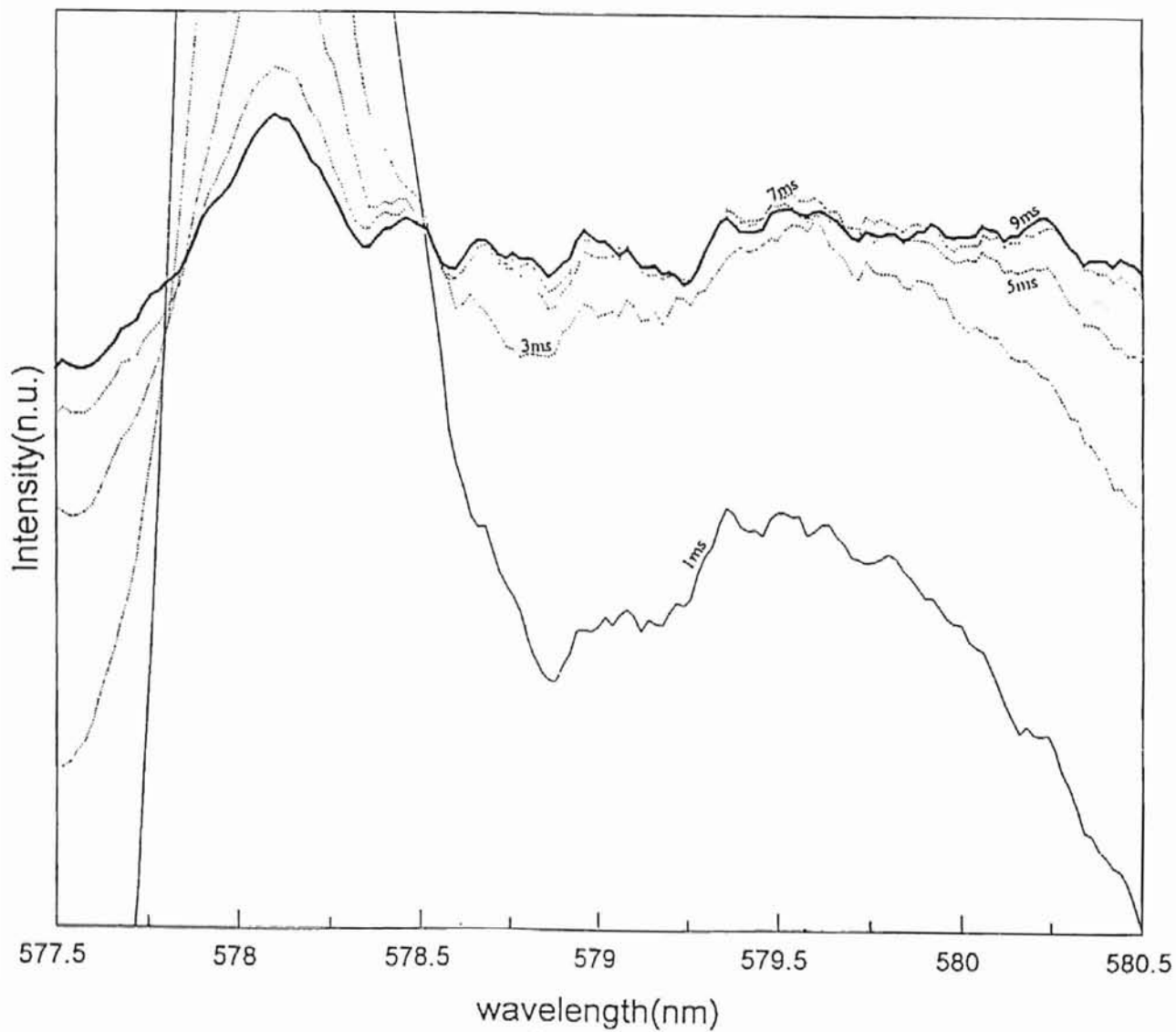


Figure 19. Fluorescence spectra of Eu^{3+} in Ca-modified glass normalized with respect to the absorption spectra. $\lambda_{\text{ex}} = 578\text{nm}$.

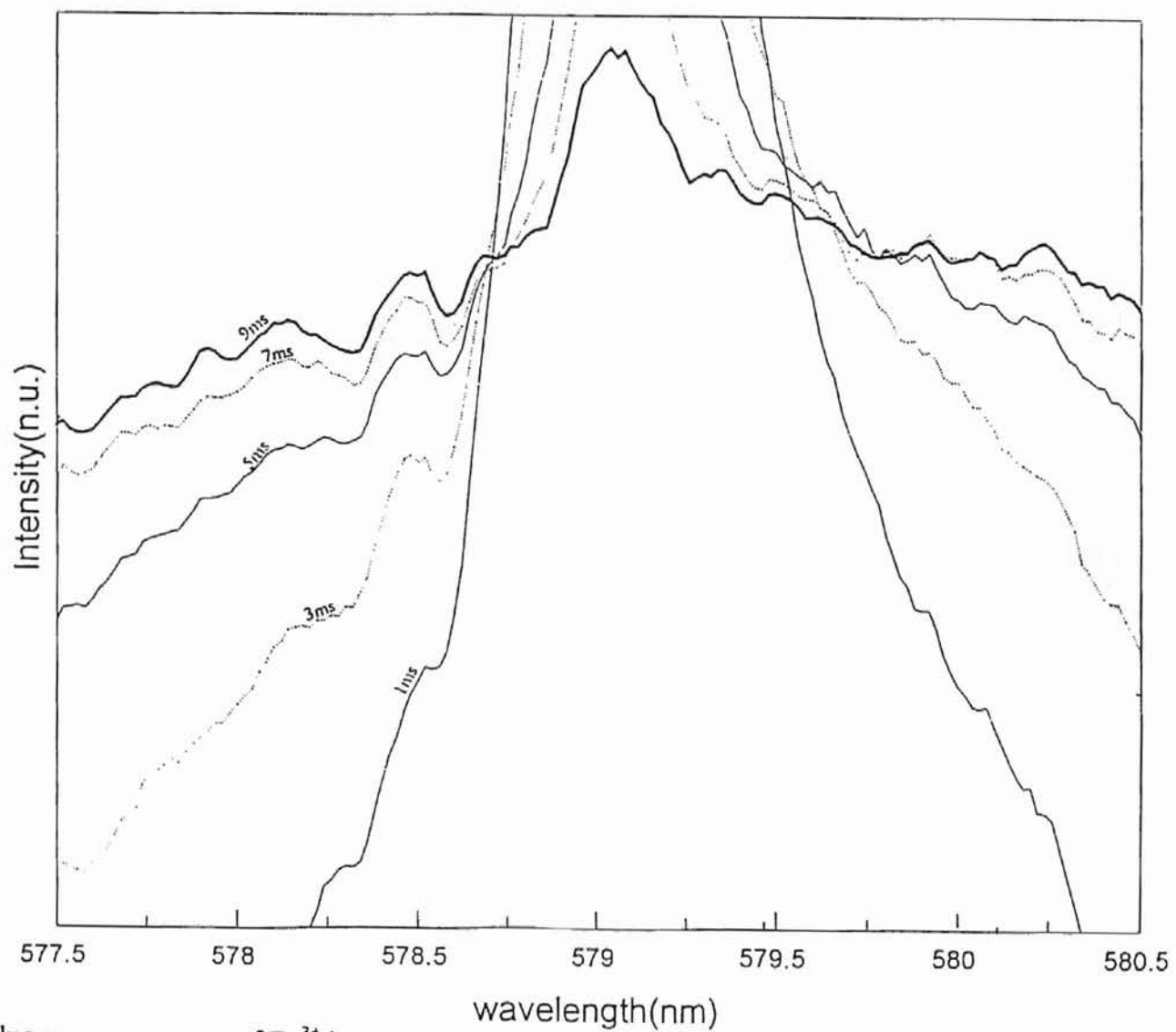


Figure 20. Fluorescence spectra of Eu^{3+} in Ca-modified glass normalized with respect to the absorption spectra. $\lambda_{\text{ex}} = 579\text{nm}$.

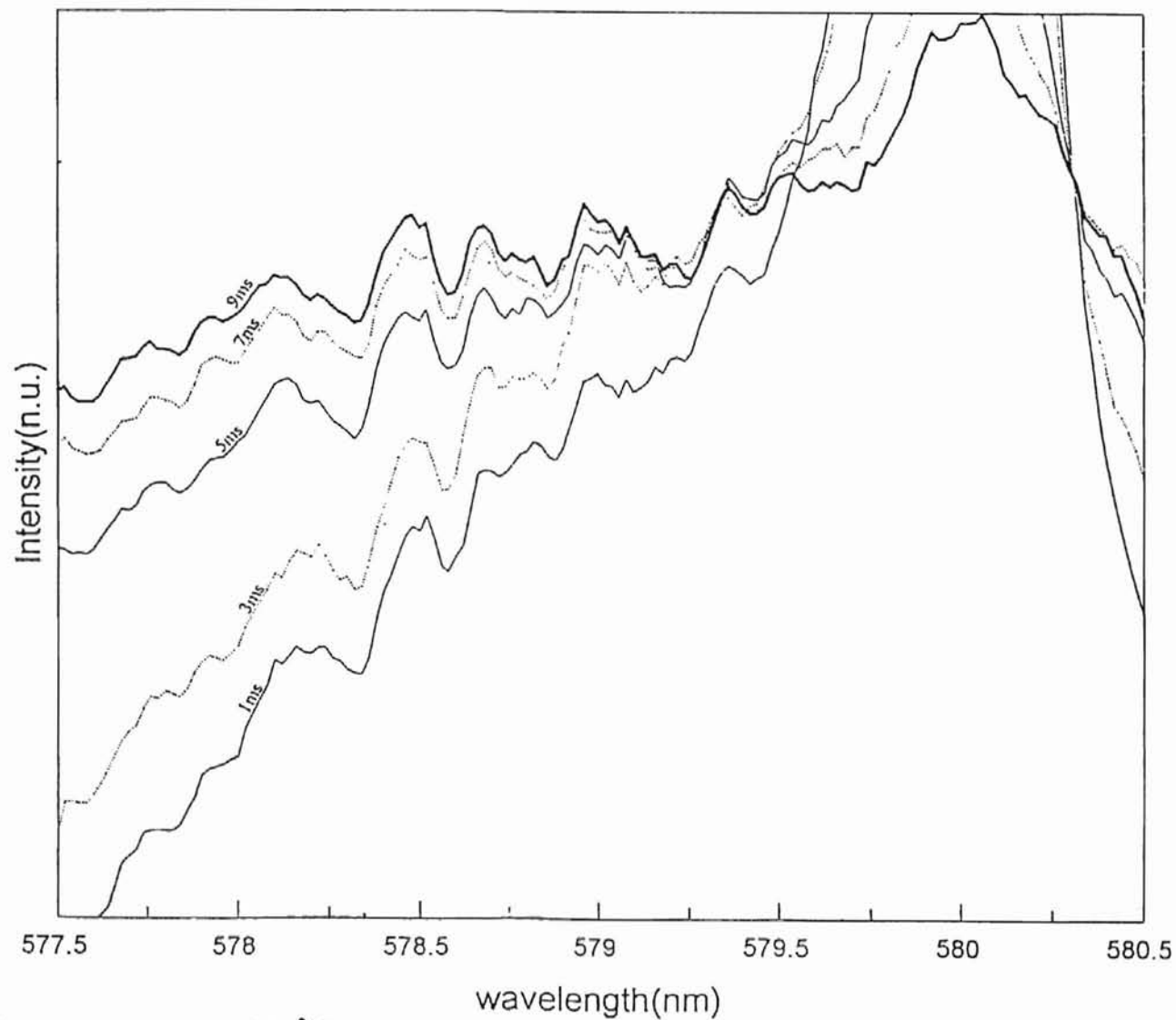


Figure 21. Fluorescence spectra of Eu^{3+} in Ca-modified glass normalized with respect to the absorption spectra. $\lambda_{\text{ex}} = 580\text{nm}$.

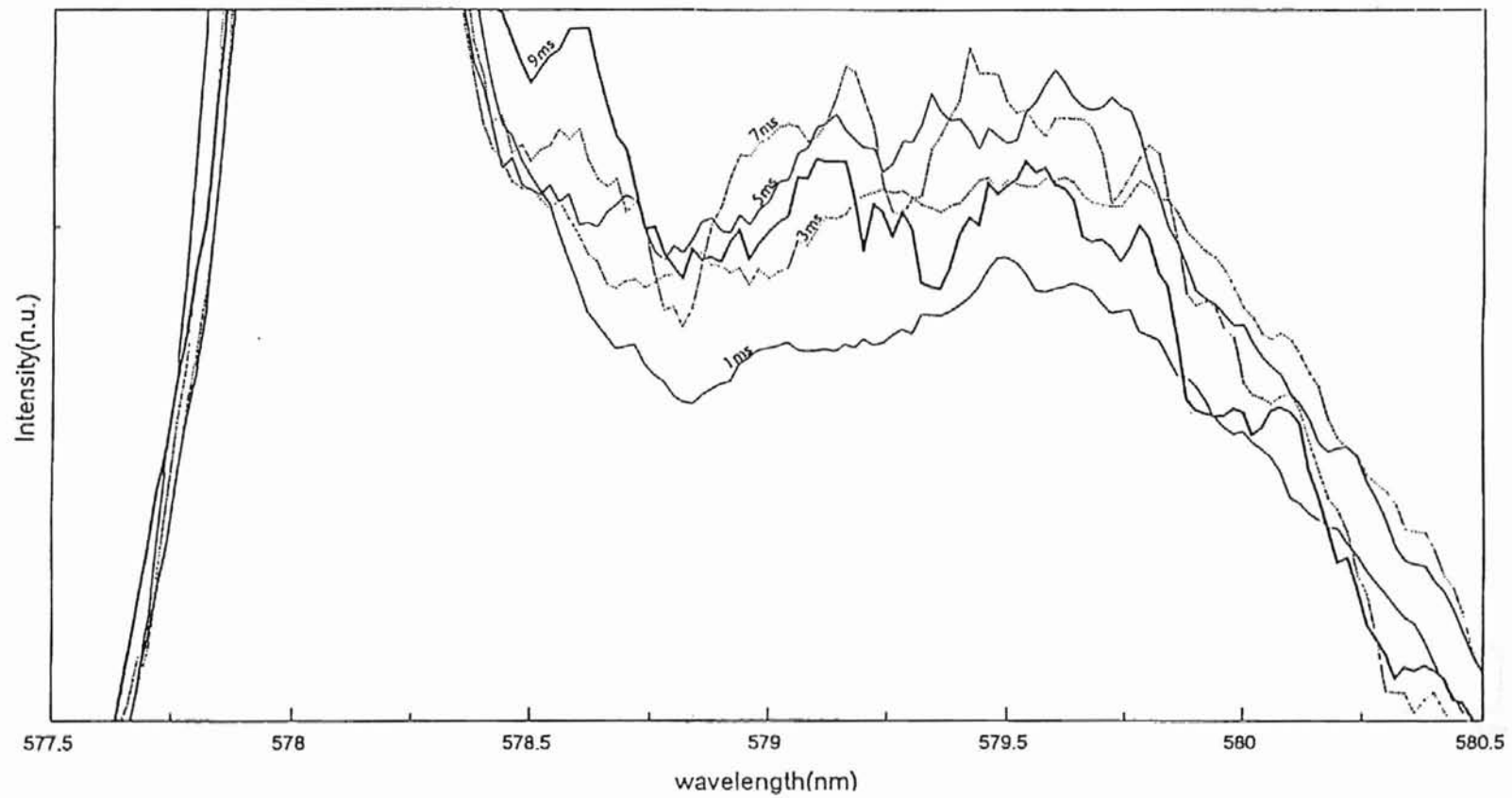


Figure 22. Fluorescence spectra of Eu³⁺ in Mg-modified glass normalized with respect to the absorption spectra. $\lambda_{ex}=578\text{nm}$.

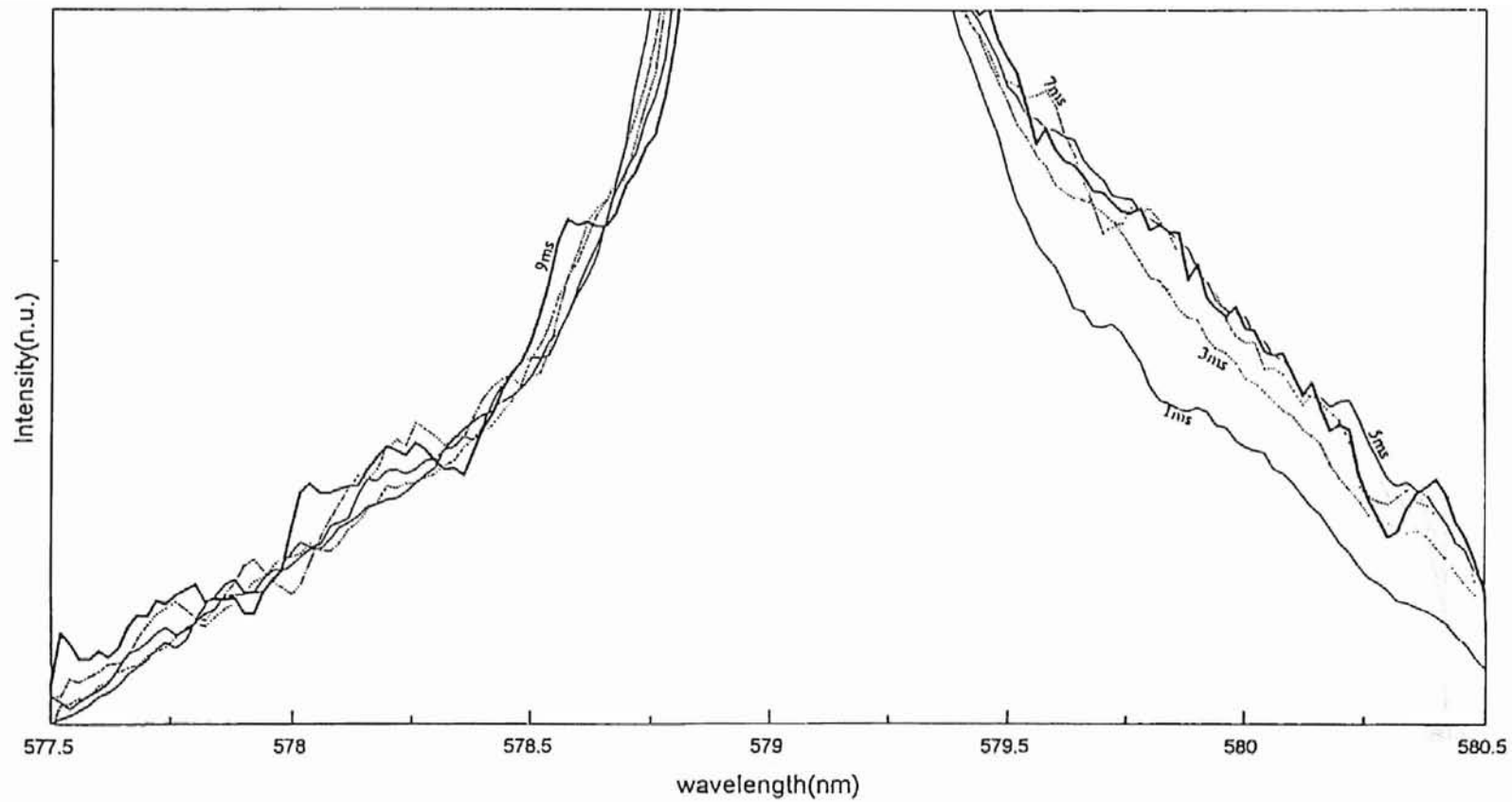


Figure 23. Fluorescence spectra of Eu³⁺ in Mg-modified glass normalized with respect to the absorption spectra. $\lambda_{ex}=579\text{nm}$.

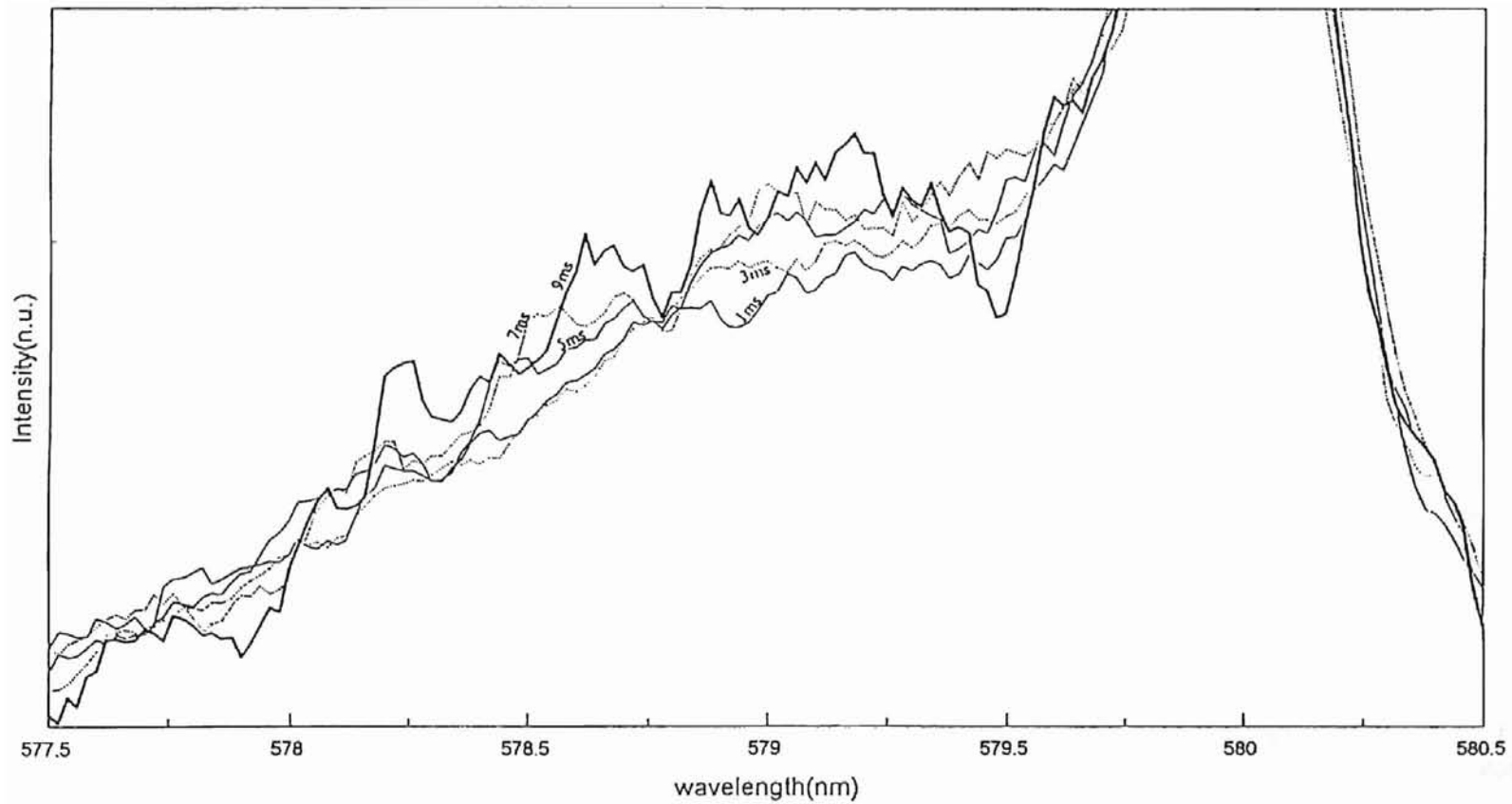


Figure 24. Fluorescence spectra of Eu³⁺ in Mg-modified glass normalized with respect to the absorption spectra. λ_{ex} = 580nm.

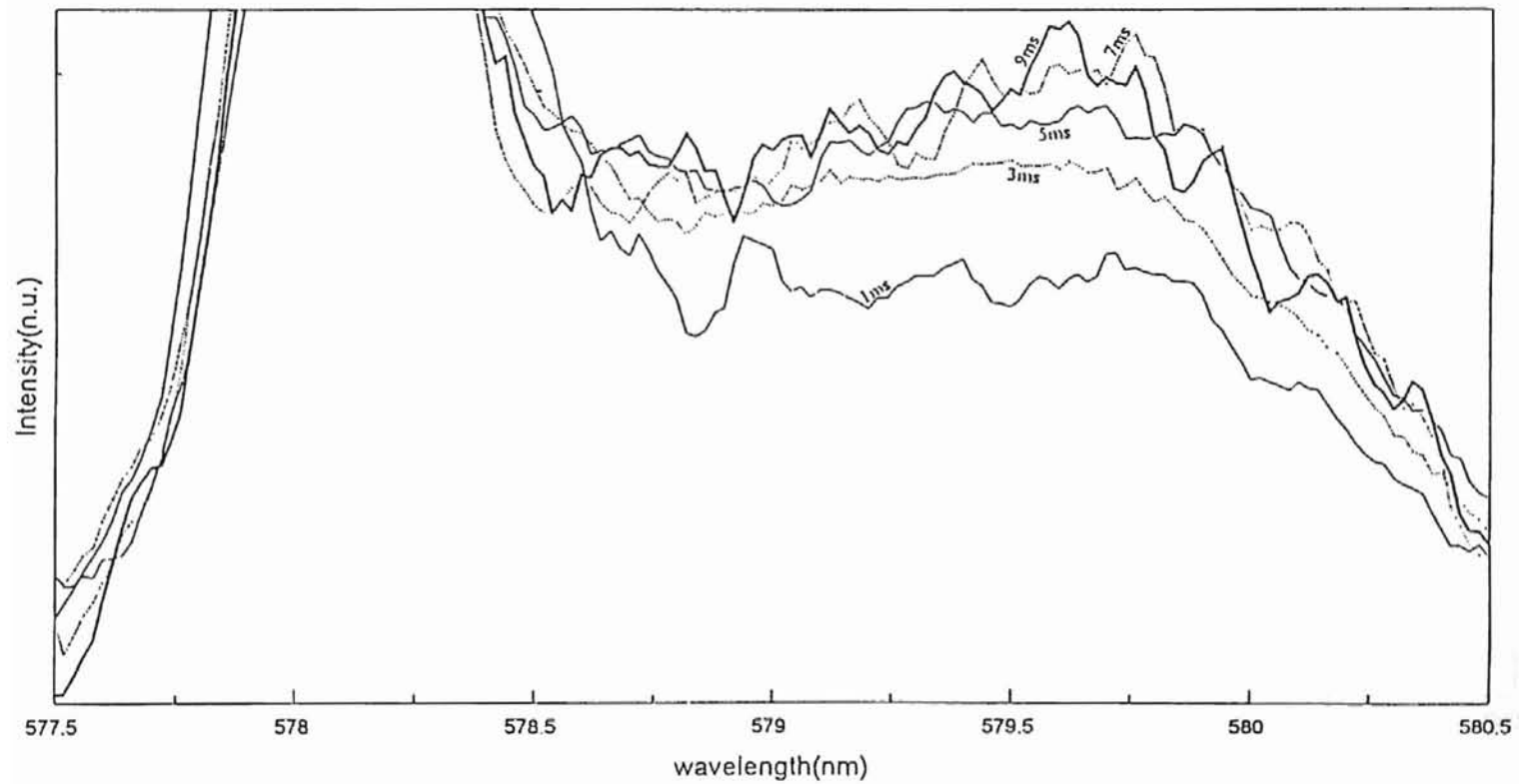


Figure 25. Fluorescence spectra of Eu³⁺ in Sr-modified glass normalized with respect to the absorption spectra. λ_{ex} = 578nm.

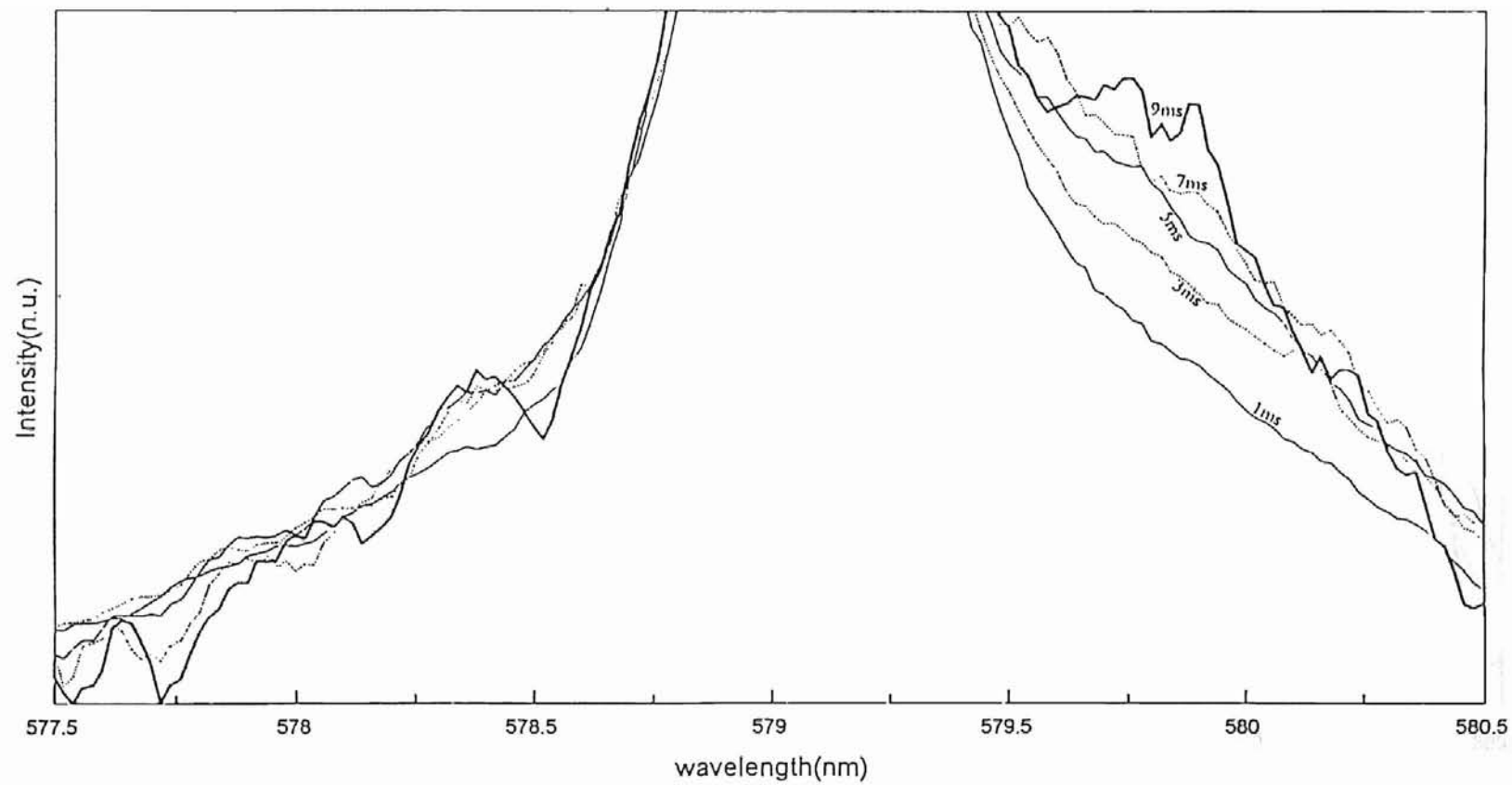


Figure 26. Fluorescence spectra of Eu³⁺ in Sr-modified glass normalized with respect to the absorption spectra. $\lambda_{ex}=579\text{nm}$.

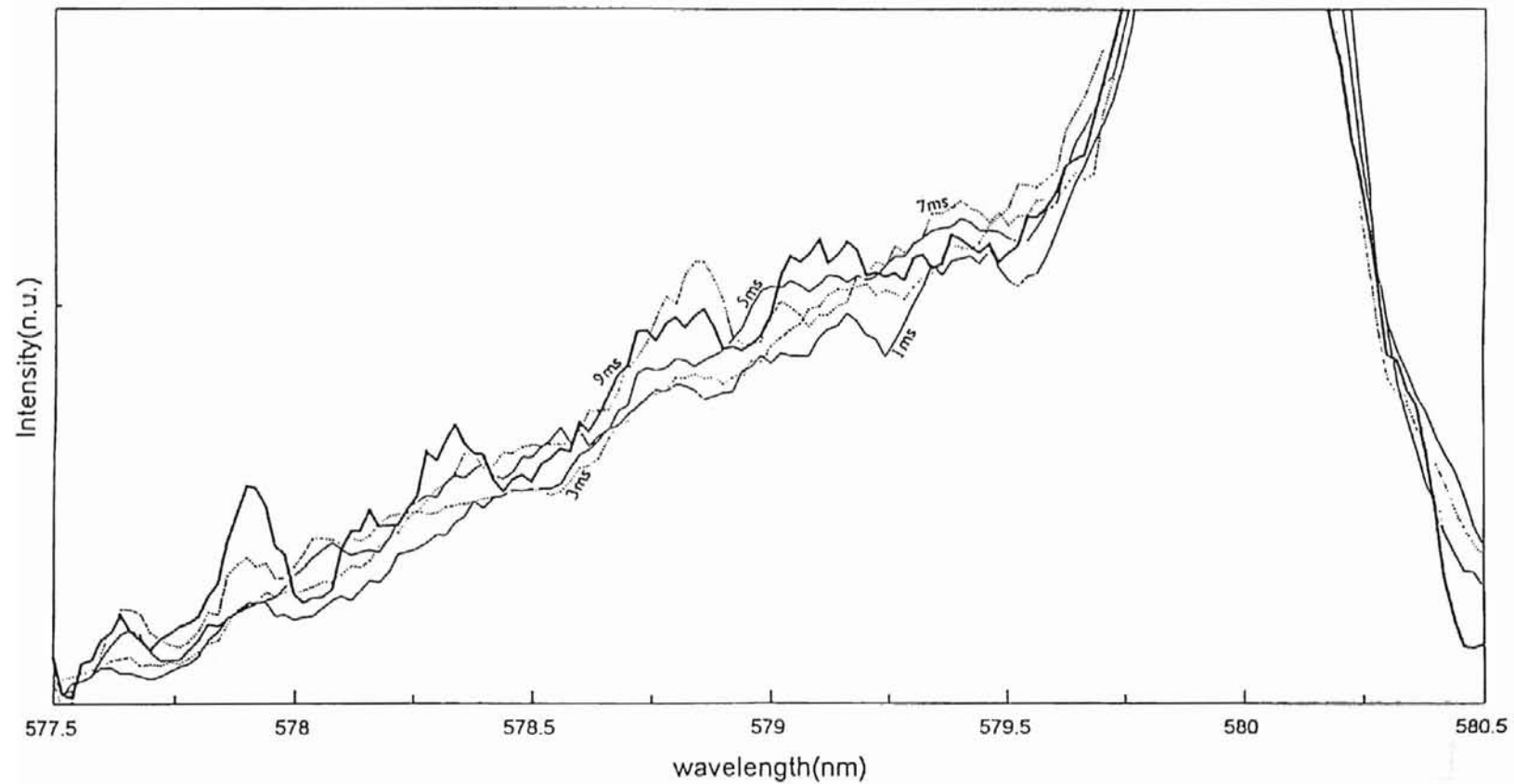


Figure 27. Fluorescence spectra of Eu^{3+} in Sr-modified glass normalized with respect to the absorption spectra. $\lambda_{\text{ex}} = 580\text{nm}$.

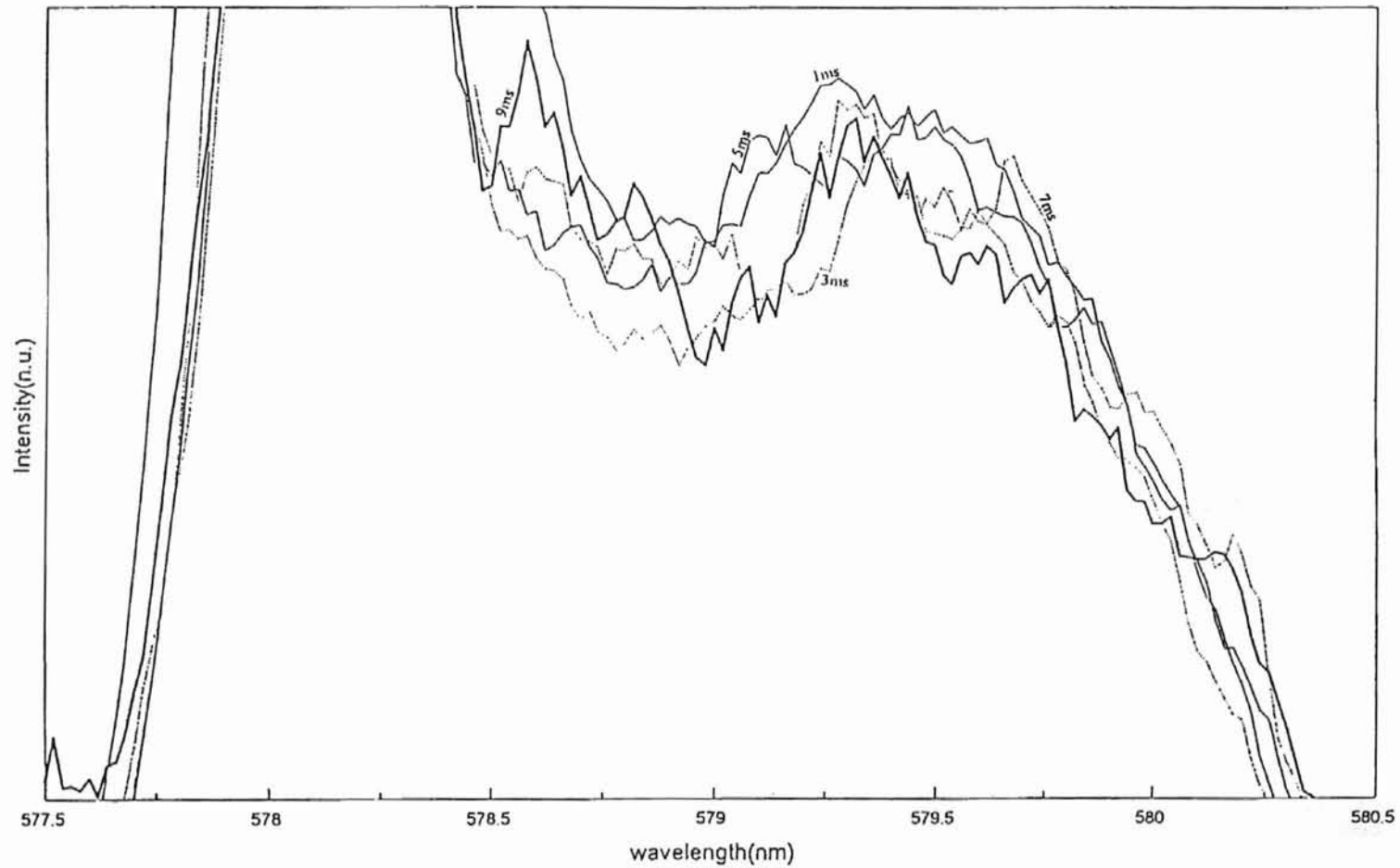


Figure 28. Fluorescence spectra of Eu^{3+} in Zn-modified glass normalized with respect to the absorption spectra. $\lambda_{\text{ex}} = 578\text{nm}$.

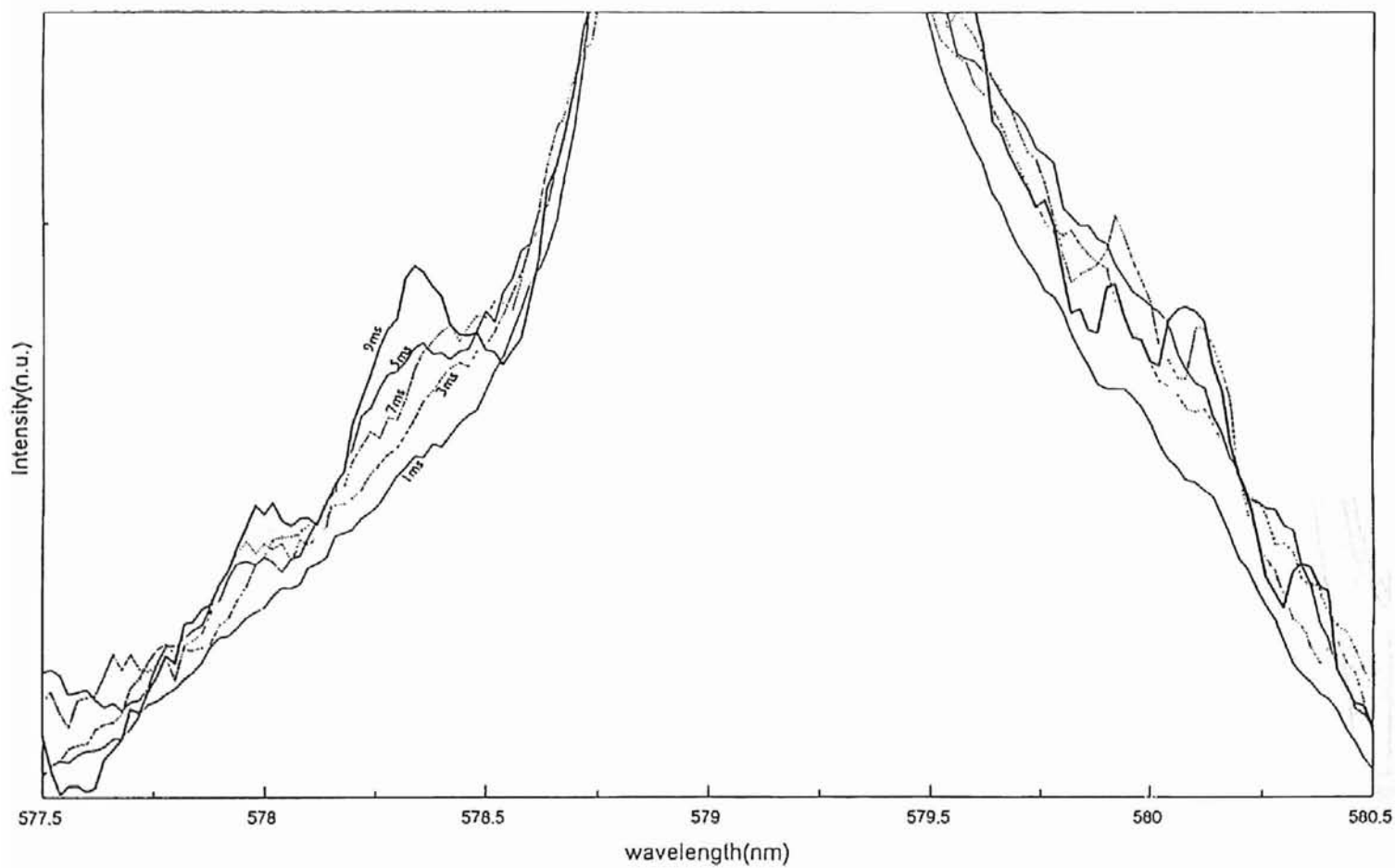


Figure 29. Fluorescence spectra of Eu^{3+} in Zn-modified glass normalized with respect to the absorption spectra. $\lambda_{\text{ex}} = 579\text{nm}$.

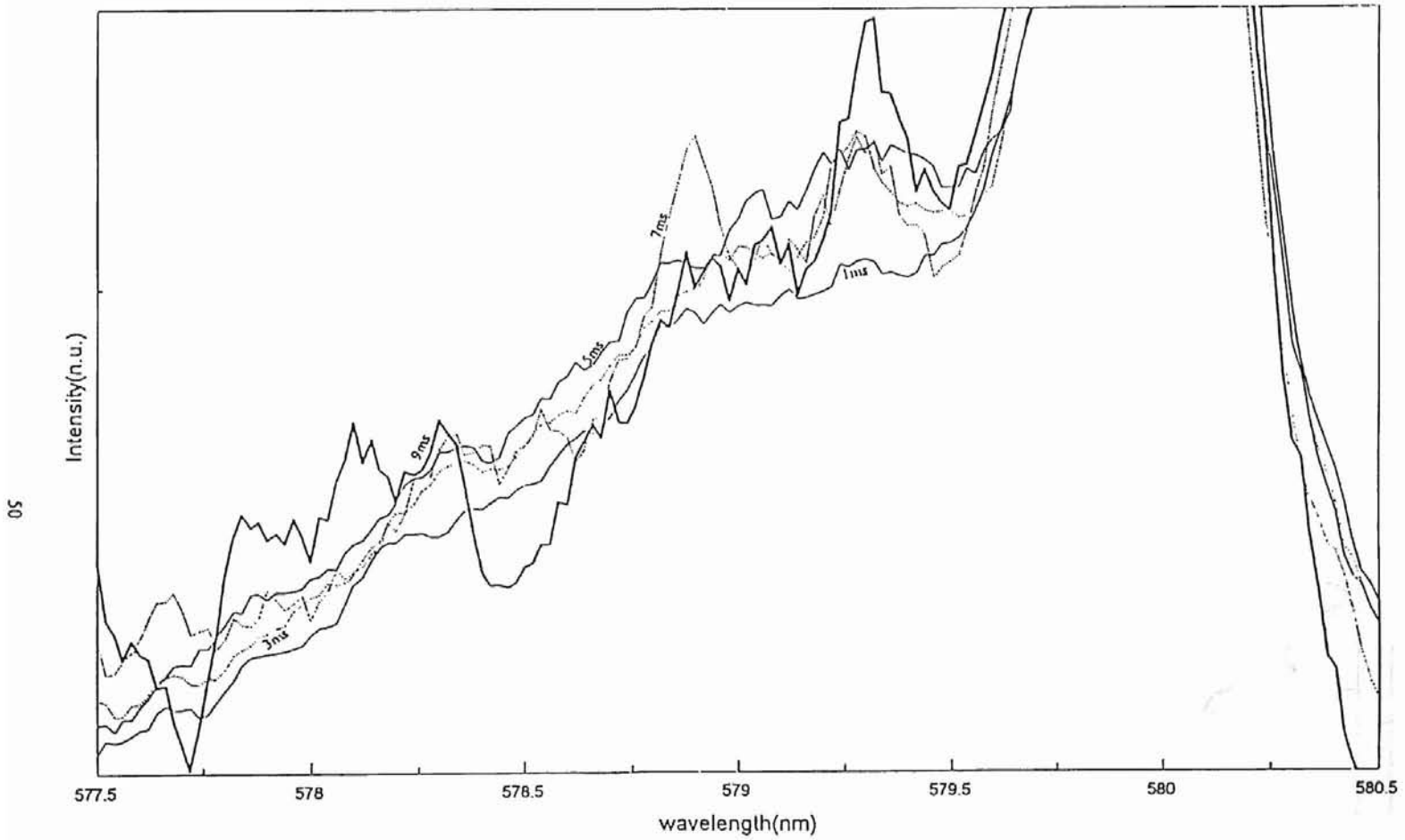


Figure 30. Fluorescence spectra of Eu^{3+} in Zn-modified glass normalized with respect to the absorption spectra. $\lambda_{\text{ex}} = 580\text{nm}$.

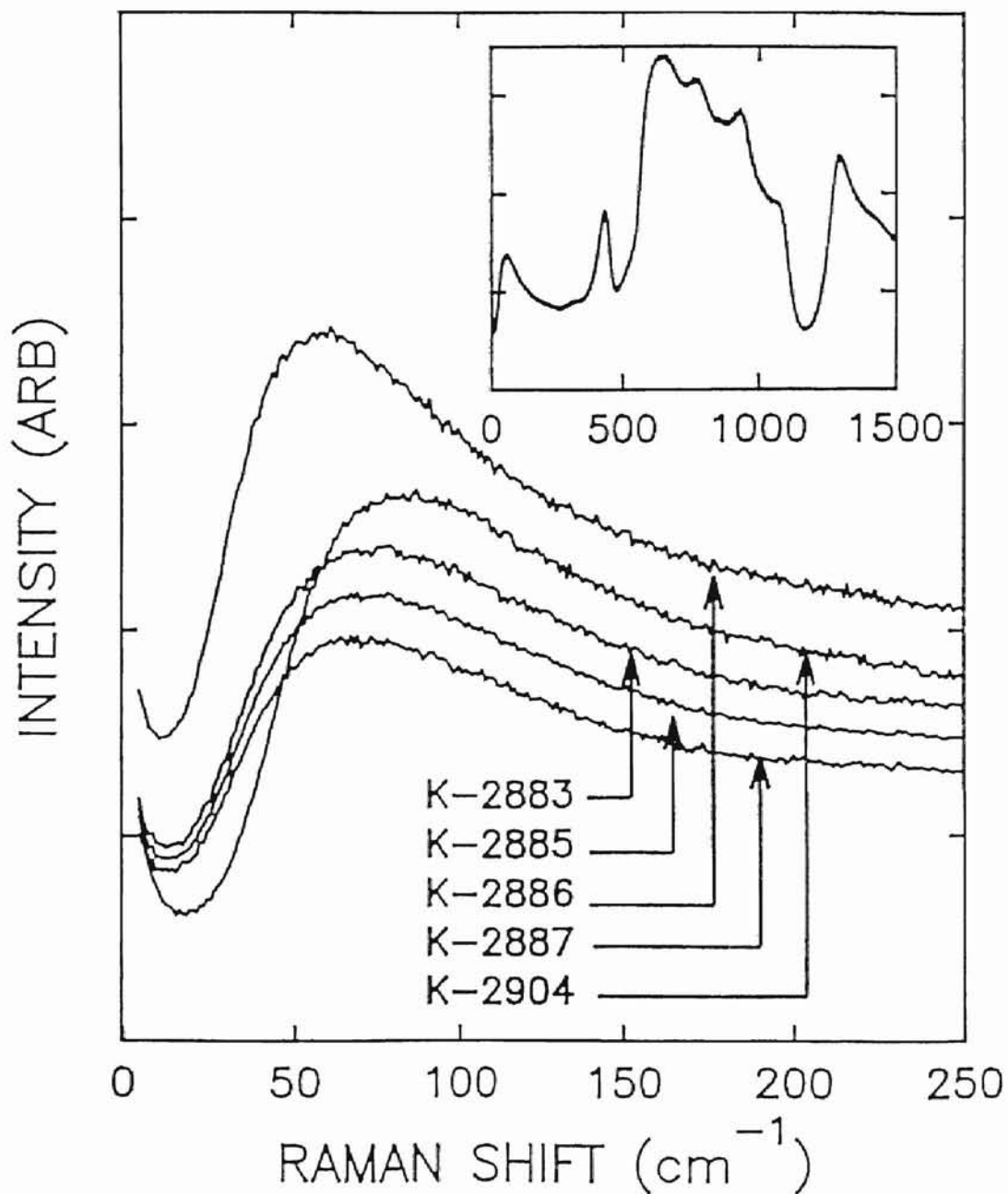


Figure 31. Raman Shift for Mg-, Ca-, Sr-, and Zn-modified glasses, with K-2883, K-2885, K-2887, and K-2904, respectively as sample names. Inset shows peaks including the low frequency Boson peak.

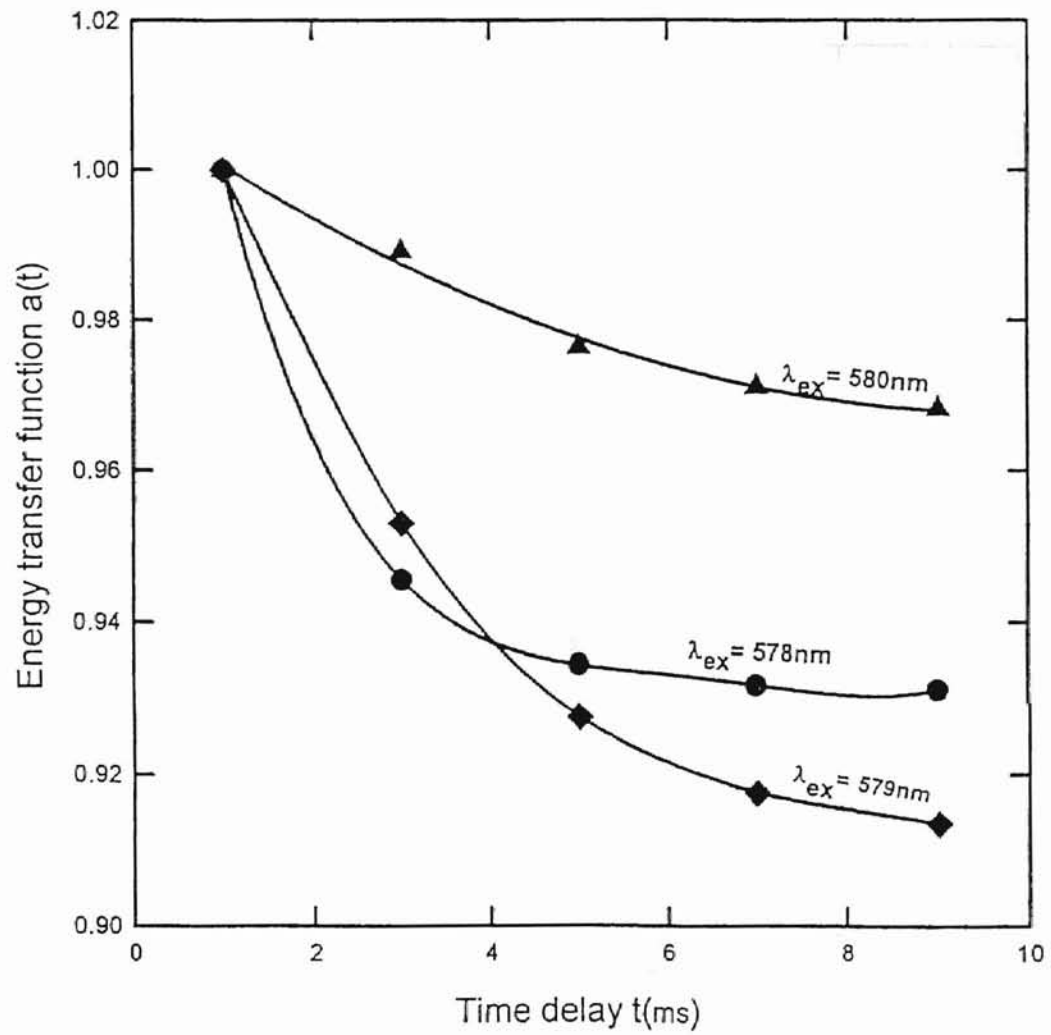


Figure 32. Time dependence of the energy transfer function defined by Eq. (6) for Ca-modified glass.

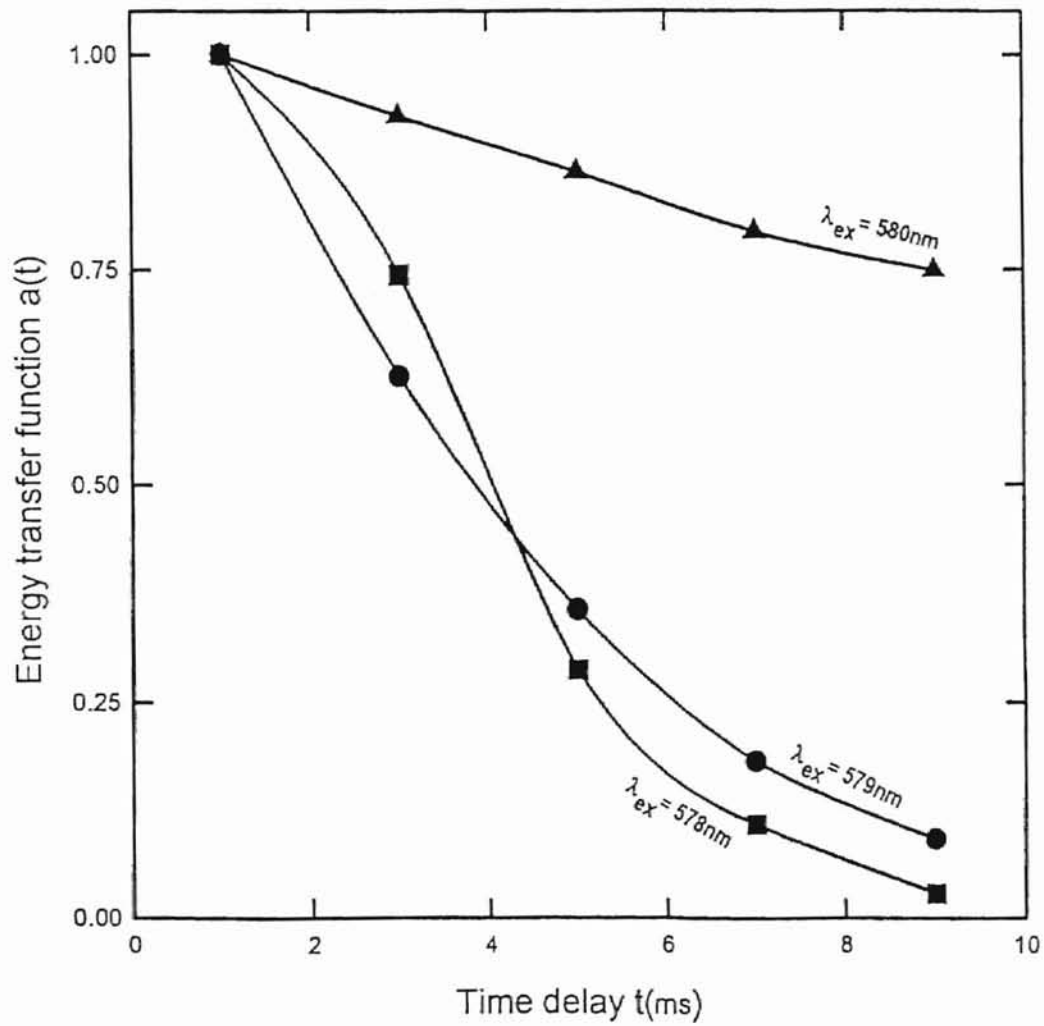


Figure 33. Time dependence of the energy transfer function defined by Eq. (6) for **Mg**-modified glass.

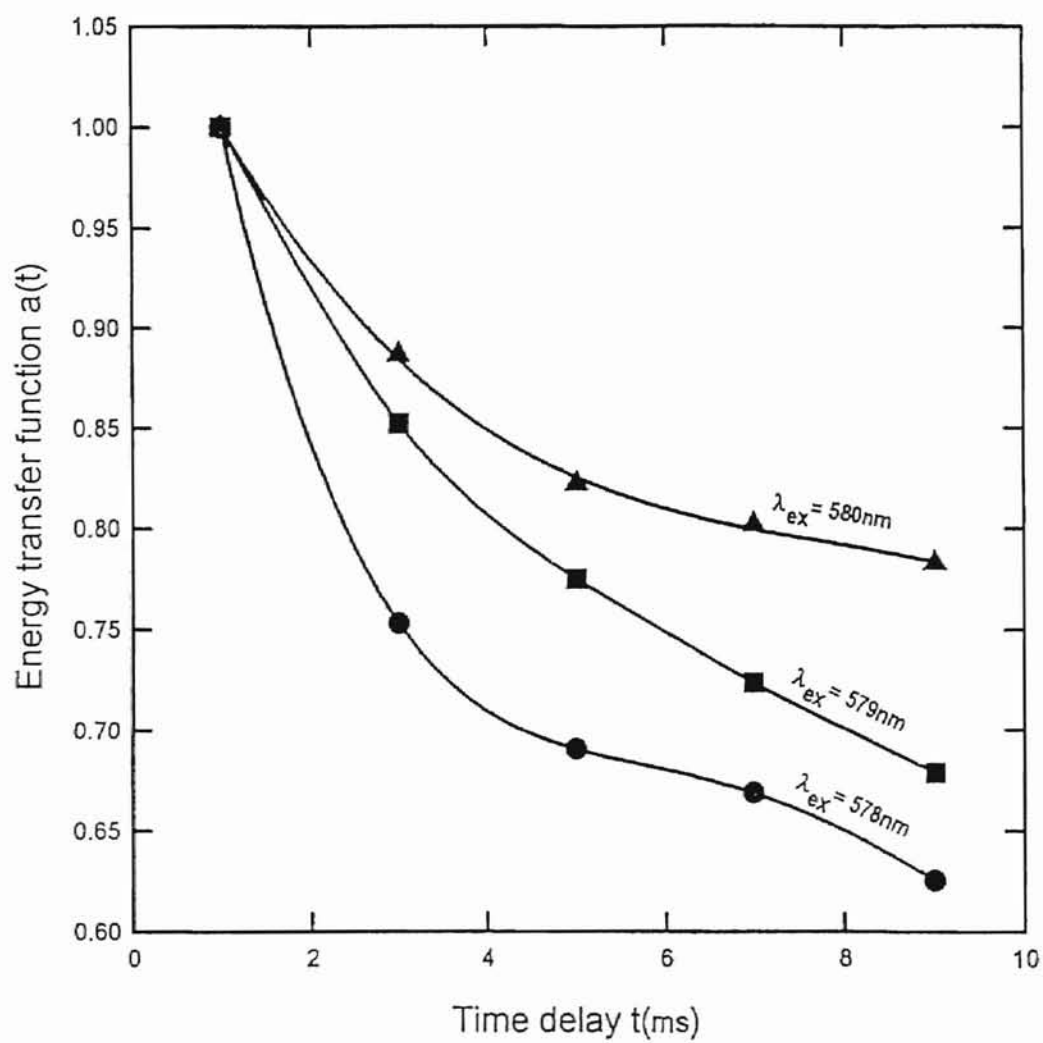


Figure 34. Time dependence of the energy transfer function defined by Eq. (6) for Sr-modified glass.

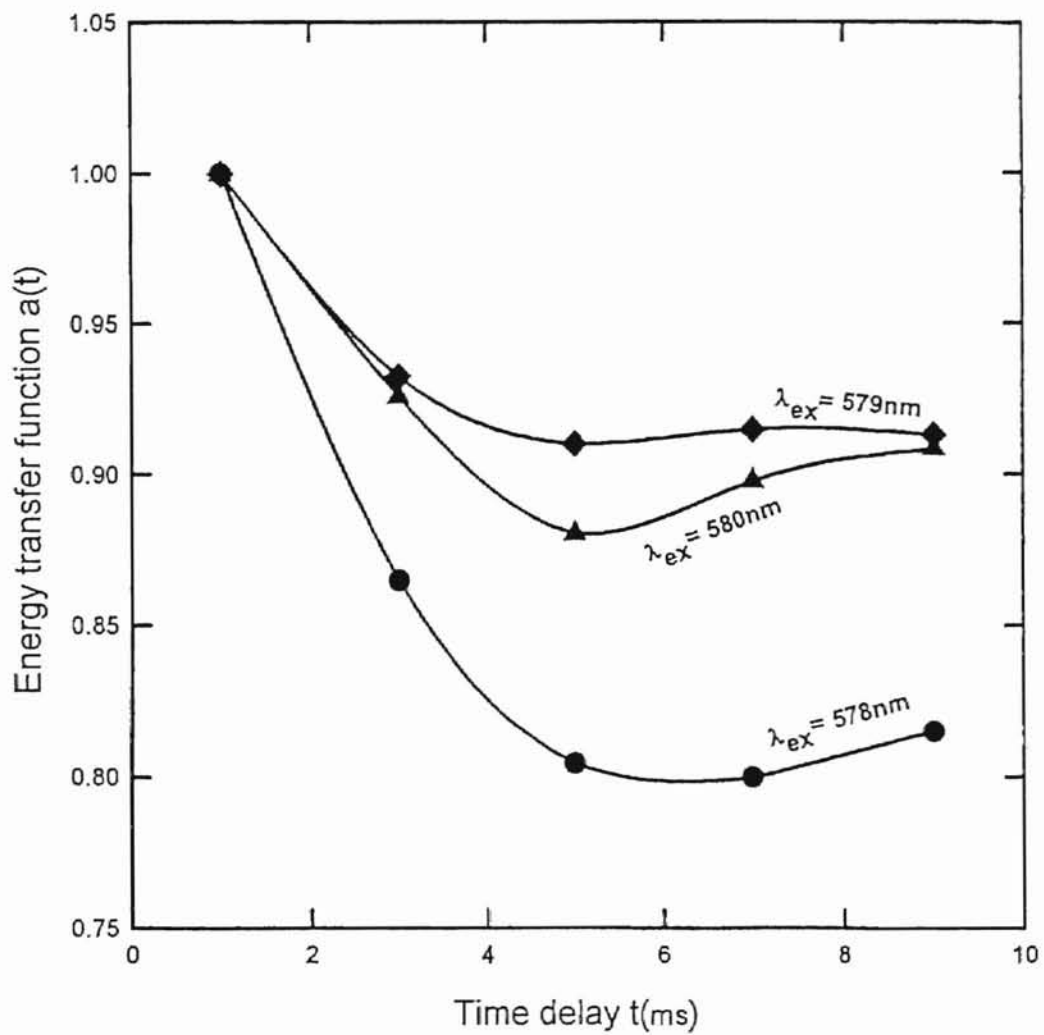


Figure 35. Time dependence of the energy transfer function defined by Eq. (6) for **Zn**-modified glass.

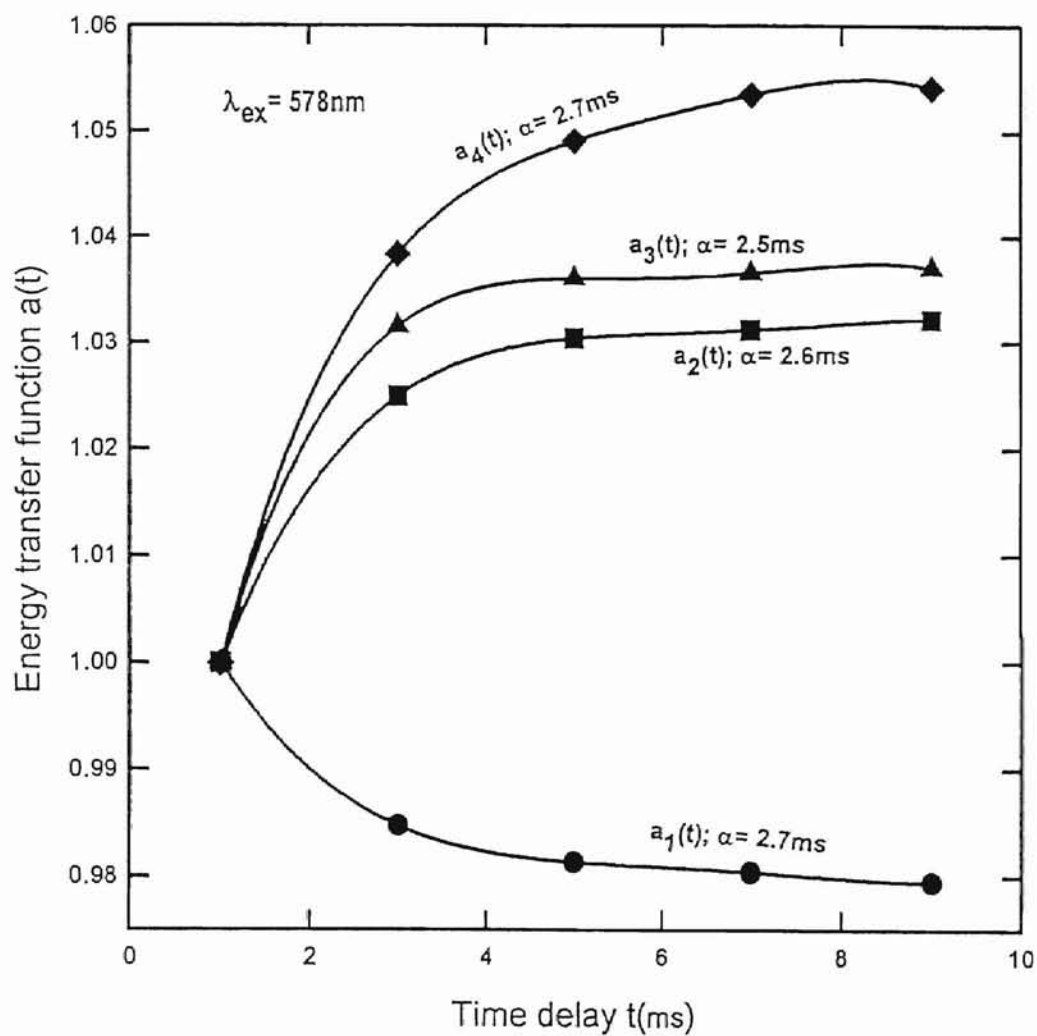


Figure 36. Time dependence of the energy transfer function for the secondary peaks numbered in order of their distance from the excitation peak in Ca-modified glass, α being the characteristic time.

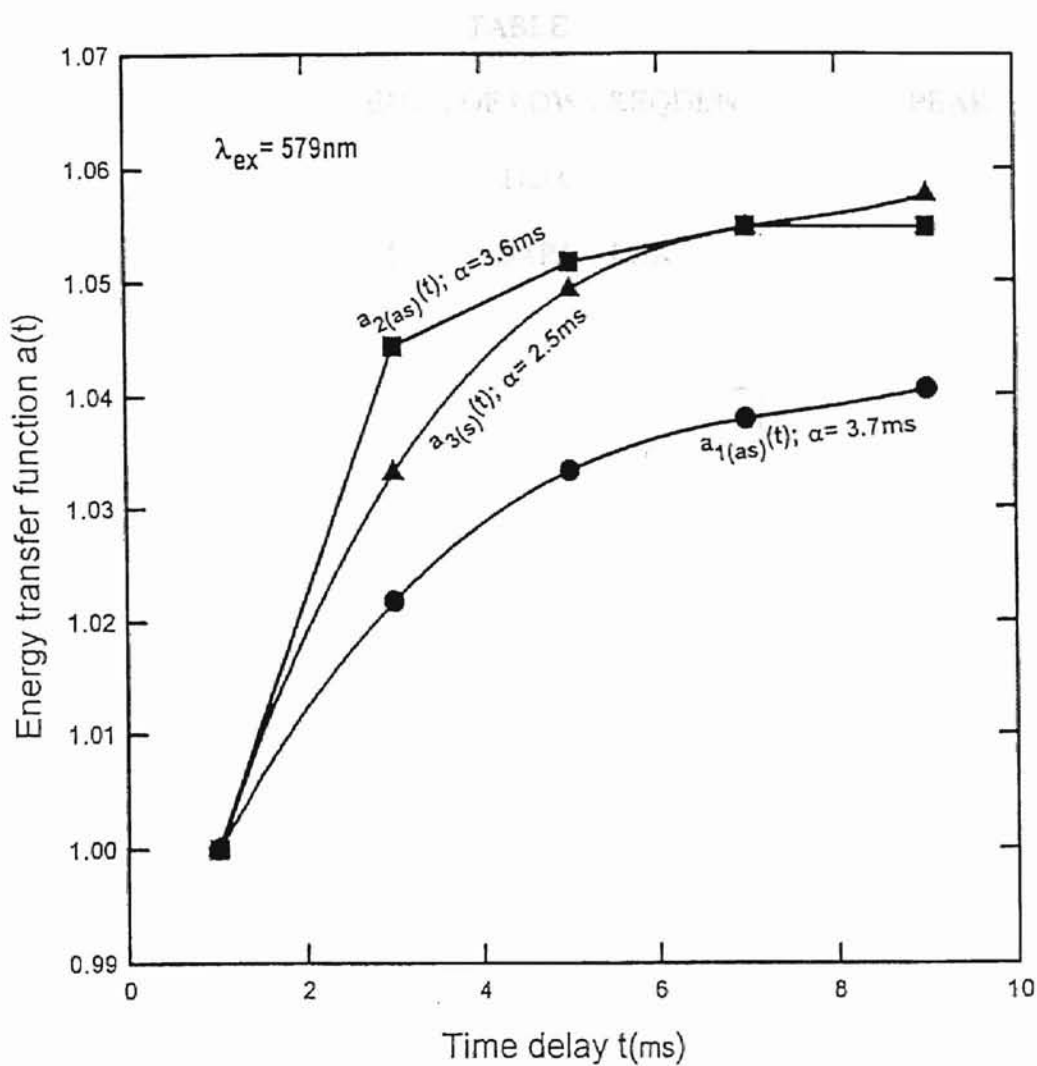


Figure 37. Time dependence of the energy transfer function for the secondary peaks numbered in order of their distance from the excitation peak in Ca-modified glass, α being the characteristic time. (as),(s) denote Stokes and anti-Stokes regions, respectively.

TABLE I
ONSET OF RISING EDGE OF LOW FREQUENCY BOSON PEAK
AND OF
SECONDARY PEAKS

Net- work Modi- fiers	Boson Peak (cm ⁻¹)	λ_{ex} (nm)	1 st peak (cm ⁻¹)	2 nd peak (cm ⁻¹)	3 rd Peak (cm ⁻¹)	4 th Peak (cm ⁻¹)
Zn	18	578	15	22	29	36
		579	15(as)	26(as), 24(s)	31(s)	43(as),39(s)
		580	15	26	37	47
Mg	12	578	11	23	32	40
		579	10(as),12(s)	20(as),21(s)	30(as)	42(as),38(s)
		580	12	22	30	38
Sr	14	578	16	27	37	44
		579	16(s), 15(as)	26(as),23(s)	37(as),34(s)	44(as),44(s)
		580	15	23	38	45
Ca	14	578	7	14	24	33
		579	8(as),8(s)	15(as), 12(s)	23(as),20(s)	34(s)
		580	-	11	22	34

* (as) and (s) denote antistokes and stokes regions, respectively.

TABLE II
ONSET OF SECONDARY PEAKS
WITH RESPECT TO 17316cm^{-1}

Zn-modified glass			Mg-modified glass		
$\lambda_{ex}=578\text{nm}$	$\lambda_{ex}=579\text{nm}$	$\lambda_{ex}=580\text{nm}$	$\lambda_{ex}=578\text{nm}$	$\lambda_{ex}=579\text{nm}$	$\lambda_{ex}=580\text{nm}$
-	9	28	-	3	20
44	19	37	47	13	29
51	-	48	55	25	38
59	37	59	65	35	50
69	-	-	73	-	60
	69			57	-
	76			66	
	84			78	
				84	

continued...

Table II continued

Sr-modified glass			Ca-modified glass		
$\lambda_{ex}=578nm$	$\lambda_{ex}=579nm$	$\lambda_{ex}=580nm$	$\lambda_{ex}=578nm$	$\lambda_{ex}=579nm$	$\lambda_{ex}=580nm$
-	7	8	-	15	15
31	14	20	25	25	25
42	25	30	33	33	33
52	35	43	41	-	40
60	-	51	52	52	52
71	62	60	66	59	-
	70	-	78	66	
	79			78	
	89				

CHAPTER IV

SUMMARY AND CONCLUSIONS

Time-resolved FLN techniques applied to the glass family under investigation yielded fluorescence spectra which became more structured with the evolution of time. The structure characterizes the rate at which the energy is transferred from one type of sites to another. Energy transfer due to preferential absorption or emission of energy according to the local energy level separations of the Eu^{3+} ions, or correlation effect is thought to cause the observed discrete structure.

However, for conservation of energy, a mode of energy transfer different from that due to correlation effect becomes necessary. This occurs for phonon energies beyond a threshold energy corresponding to the frequency at the mobility edge, which has been taken as one at the onset of low frequency Boson peak (fig. 31).

A common spectral feature observed in all the scans is that at a fixed frequency interval away from the central resonant peak, a secondary peak appears; away from this secondary peak at the same frequency separation, another secondary peak appears, and so on. This is an indication of energy transfer due to localized phonons being effective when the energy separation between the excited states of different sites corresponds to ω_{mc} . The secondary peaks become more structured with the evolution of time. The energy transfer function $a(t)$ for the secondary peaks rises exponentially (fig. 36-37), while it decays exponentially for the central resonant peak (fig.32-35). However, for larger times compared with the characteristic time for the exponential function, $a(t)$, the curves saturate and assume constant values, whence the influx of energy into a certain type of sites becomes comparable to its outflow from the region. Thus the analysis of fluorescence spectra for a frequency regime greater than or comparable with ω_{mc} favors energy transfer mediated by localized phonons.

REFERENCES

1. M. J. Weber, Laser Spectroscopy of Solids, eds., W. M. Yen, and P. M. Selzer, 189, (Springer, New York, 1981).
2. Xu Gang, G. Boulon, and R. C. Powell, J. Chem. Phys. **78**(7), 4374(1983).
3. Xu Gang, and R. C. Powell, J. Applied Physics, **57**(4), 1299(1985).
4. G. S. Dixon, Diffusion and Defect Data, **53-54**, 133(1987).
5. G. S. Dixon, J. Luminescence, **45**, 93(1990).
6. M. J. Weber, J. Hegarty, and W. M. Yen, Physical Review B, **18**(10), 5816(1978).
7. C. Brecher, and L. A. Riseberg, Physical Review B, **21**(6), 2607(1980).
8. S.A. Brawer and M. J. Weber, Appl. Phys. Lett. **35**(1), 31(1979).
9. V.D. Frichette, (ed.), Non-Crystalline Solids, John Wiley & Sons, Inc. 1960.
10. R. Zallen, The Physics of Amorphous Solids, John Wiley & Sons, Inc., 1983.
11. C. Kittel, Introduction to Solid State (6th edition), John Wiley & Sons, Inc., 1986.
12. G. S. Dixon, B. D. Gault, S. Shi, P. A. Watson, and J. P. Wicksted, Physical Review B, Vol. 49, No. 1, 257(1994).
13. O. Entin-Wohlman, Condensed Matter Physics, The Theodore D. Holstein Symposium, ed. R. L. Orbach, 160(1986).
14. T. Holstein, S. K. Lyo, and R. Orbach, in: Laser Spectroscopy of Solids, eds. W. M. Yen and P. M. Selzer (Springer, New York, 1981), p. 39.
15. G. S. Dixon, X. Gang, and R. C. Powell, Phys. Rev. **B33** (1986)2713; J. Phys. (Paris) **10**(1985) C7-331; F. Durville, G. S. Dixon, and R.C. Powell, J. Lumin.**36**(1987)221.
16. S. Kojima, Jpn. J. Appl. Phys. Vol. 32(1993).
17. N. Garcia, E. Duval, A. Boukenter, and J. Serughetti, J. Chem. Phys. **99**(3), 2040 (1993).
18. T. Achibat, A. Boukenter, and E. Duval, J. Chem. Phys. **99**(3), 2046(1993).
19. S. Alexander, O. Entin-Wohlman, and R. Orbach, Phys. Rev. B, **34**, 2726(1986).
20. D.G. Cahill, and P.O. Pohl, Ann. Rev. Phys. Chem., 93(1988).

21. A. Jagannathan, R. Orbach, and O. Entin-Wohlman, *Physical Review B*, **39**(18), 13465(1989).
22. C. R. A. Catlow (ed.), *Defects and Disorder in Crystalline and Amorphous Solids, Series C: Mathematical and Physical Sciences*, **418**, Kluwer Academic Publishers, 1991.
23. W.A. Phillips, (ed.), *Topics in Current Physics, Amorphous Solids, Low Temperature Properties*, Springer-Verlag, 1981.
24. J. M. Ziman, *Electrons and Phonons*, Clarendon Press, Oxford, 1960.
25. Allen Corney, *Atomic and Laser Spectroscopy*, Oxford University Press, 1977.
26. George H. Atkinson, (ed.), *Time Resolved Vibrational Spectroscopy*, Academic Press Inc., 1983.
27. V. Sychra, V. Svoboda, and, I. Rubiska, *Atomic Fluorescence Spectroscopy*, Van Nostrand Reinhold Company Ltd., 1975.
28. W. G. Laidlaw, *Introduction to Quantum Concepts in Spectroscopy*, McGraw Hill Book Company, 1970.
29. R. Risefeld, and N. Lieblich, *J. Electrochem. Soc* **121**, 1338(1974).
30. R. Risefeld, and Eckstien, *J. Non-Cryst. Solids* **12**, 357(1973).

VITA

Sheena Jacob

Candidate for the Degree of

Master of Science

Thesis: LOCALIZED PHONON-MEDIATED ENERGY TRANSFER AMONG Eu^{3+}
IONS IN SILICATE GLASS-HOSTS

Major Field: Physics

Biographical:

Personal Data: Born in Ernakulam, Kerala, India, on April 12, 1963, the daughter of Jacob George and Omana Jacob.

Education: Graduated from Birla Balika Vidyapeeth, Pilani, Rajasthan, India, June 1981; received Bachelor of Science (Honors) degree in Physics from Panjab University, Chandigarh, India, June 1984; completed requirements for the Master of Science degree at Oklahoma State University, December 1995.

Professional Experience: Teaching Assistant, Department of Physics, Oklahoma State University, August 1993 to May 1995.